Clim. Past Discuss., doi:10.5194/cp-2015-177, 2016
Manuscript under review for journal Clim. Past
Published: 26 January 2016


# A record of Neogene seawater $\delta^{11}B$ reconstructed from paired $\delta^{11}B$ analyses on benthic and planktic foraminifera.

Greenop R.[1,2*], Foster, G.L.[1], Sosdian, S.M.[3], Hain, M.P.[1], Oliver, K.I.C.[1], Goodwin, P.[1], Chalk, T.B.[1,4], Lear, C.H.[3], Wilson, P.A.[1]

[*]Corresponding author

[1] *National Oceanography Centre Southampton, University of Southampton, Waterfront Campus, European Way, Southampton SO14 3ZH, UK*

[2]*School of Geography & Geosciences, Irvine Building, University of St Andrews, North Street, St Andrews, KY16 9AL, UK*

[3]*School of Earth & Ocean Sciences, Cardiff University, Cardiff, CF10 3AT, UK*

[4] *Department of Physical Oceanography, Woods Hole Oceanographic Institution, Woods Hole, Massachusetts, USA*

## Abstract:

The boron isotope composition ($\delta^{11}B$) of planktic foraminiferal calcite, which reflects seawater pH, is a well-established proxy for reconstructing palaeo- atmospheric $CO_2$ and seawater carbonate chemistry. However, to translate $\delta^{11}B$ measurements determined in calcareous fossils into pH we need to know the boron isotope composition of the parent seawater ($\delta^{11}B_{sw}$). While a number of $\delta^{11}B_{sw}$ reconstructions exist, the discrepancies between them reveals uncertainties and deficiencies that need to be addressed. Here we present a new $\delta^{11}B_{sw}$ record based on the $\delta^{11}B$ difference between planktic and benthic foraminifera and an estimate of the pH gradient between surface and deep water. We then calculate $\delta^{11}B_{sw}$ two different ways. One variant of our method assumes that the pH gradient between surface and deep has remained the same as today over the past 23 Ma; the other uses the $\delta^{13}C$ gradient between surface and deep to represent change in the pH gradient through time. The results of these two methods of calculating $\delta^{11}B_{sw}$ are broadly consistency with each other, however, based on extensive carbon cycle modelling using CYCLOPS and

Clim. Past Discuss., doi:10.5194/cp-2015-177, 2016
Manuscript under review for journal Clim. Past
Published: 26 January 2016


GENIE we favour the $\delta^{13}C$ gradient method. In our favoured $\delta^{11}B_{sw}$ reconstruction, $\delta^{11}B_{sw}$ is around 2 ‰ lower than today at ~ 37.5 ‰ during the early and middle Miocene and increases to the modern value (39.61 ‰) by ~ 5 Ma. A similar pattern of change is evident in the seawater composition of three other stable isotope systems, Mg, Li and Ca. Concurrent shifts in the seawater isotopic composition of all four of these elements during the late Miocene, suggest a common forcing mechanism. We hypothesise the most likely cause of these shifts is a change in the isotopic composition of the riverine input, potentially driven by an increase in secondary mineral formation since ~15 Ma.

## 1. Introduction

Key to determining the relationship between $CO_2$ and climate in the geological past is the calculation of reliable estimates of absolute $CO_2$ through time. In recent years the boron isotope composition ($\delta^{11}B$) of foraminiferal calcite has become one of the most commonly used tools to reconstruct $CO_2$ beyond the last 800 kyrs and throughout the Cenozoic Era (Foster, 2008; Hönisch et al., 2009; Pearson et al., 2009; Bartoli et al., 2009; Foster et al., 2012; Badger et al., 2013; Henehan et al., 2013; Greenop et al., 2014; Martìnez-Botì, et al., 2015a). Yet long-term change in the boron isotope composition of seawater ($\delta^{11}B_{sw}$) is poorly constrained and represents a major source of the uncertainty associated with $\delta^{11}B$-determined $CO_2$ estimates. In the modern ocean boron is a conservative element with a spatially invariant isotope ratio (39.61‰; Foster et al., 2010), but this value is subject to change through geological time. The residence time of boron in the ocean is estimated to lie between 11 and 17 Myrs (Lemarchand et al., 2002). Therefore we can expect the uncertainty associated with $\delta^{11}B_{sw}$ to be an important factor in $CO_2$ estimates beyond the late Pliocene (~ 4-5 Ma, Palmer et al., 1998; Pearson et al., 2009; Foster et al., 2012).

The ocean boron budget and its isotopic composition are controlled by a number of inputs and outputs (Fig. 1). However, because the magnitude of the boron fluxes between land, the ocean and the atmosphere are still poorly understood, the residence time and changes in both concentration ($[B]_{sw}$) and isotopic composition ($\delta^{11}B_{sw}$) through time remain uncertain. The main inputs of B into the ocean are silicate weathering delivered to the ocean by rivers (Lemarchand et al., 2002), hydrothermal

Clim. Past Discuss., doi:10.5194/cp-2015-177, 2016
Manuscript under review for journal Clim. Past
Published: 26 January 2016


vents (You et al., 1993) and fluid expelled from accretionary prisms (Smith et al., 1995). The major outputs are oceanic crust alteration (Smith et al., 1995), adsorption onto sediments (Spivack and Edmond, 1987) and co-precipitation into carbonates (Hemming and Hanson, 1992). In all three cases the light $^{10}B$ isotope is preferentially removed such that seawater is isotopically heavier (39.61‰) than the inputs (which average at 10.4‰). Atmospheric boron may also be an important flux both into and out of the ocean (Park and Schlesinger, 2002). While some studies have suggested that precipitation within the catchment area may be an important factor controlling the $\delta^{11}B$ in rivers (Rose-Koga et al., 2006), other studies have shown atmospheric boron to be a secondary control on riverine boron isotope composition (Lemarchand and Gaillardet, 2006).

Unlike many other isotopic systems (e.g. Mg, Ca, Li, Sr) to date no archive has been discovered that simply records unaltered seawater $\delta^{11}B$. This is a result of the pH dependency of B speciation in seawater upon which the $\delta^{11}B$-pH proxy is based (Zeebe and Wolf-Gladrow, 2001) and imparts a pH dependency on all marine precipitates so far examined. Empirical reconstructions of $\delta^{11}B_{sw}$ must therefore use "indirect" approaches; so far four methods have been applied to the Cenozoic (0-65 Ma) (Fig. 2). Firstly, geochemical modelling of the changes in the flux of boron into and out of the ocean through time has been used to suggest that the $\delta^{11}B_{sw}$ increased from 37‰ at 60 Ma to 40‰ ± 1‰ today (Lemarchand et al., 2002). However, there are uncertainties associated with quantification of, and controls on, the oceanic inputs and outputs of boron (Lemarchand et al., 2002). For instance, it is possible that subtle variations in poorly constrained factors such as oceanic crustal permeability, the lifetime of water-rock interactions and the expansion rate of the oceanic ridge can have a large effect (variations between 30‰ and 50‰ at a 10 million year scale) on the amount and isotopic composition of the boron removed from the ocean during oceanic crust alteration (Simon et al., 2006). These issues coupled with uncertainties in the magnitude of the atmospheric boron flux (Park and Schlesinger, 2002), make direct geochemical modelling of the evolution of $\delta^{11}B_{sw}$ currently under constrained at present.

The boron isotopic composition of marine halites and sea salts has also been used to reconstruct the boron isotope composition of the ocean in the past (Paris et al., 2010).

Clim. Past Discuss., doi:10.5194/cp-2015-177, 2016
Manuscript under review for journal Clim. Past
Published: 26 January 2016


Results from studies employing this method suggest that $\delta^{11}B_{sw}$ has varied by 7‰ over the Neogene (Fig. 2) (Paris et al., 2010). Yet brine-halite fractionation offsets of -20‰ to -30‰ and -5‰ are reported from laboratory and natural environments respectively casting doubt over the validity of the assumption that no fractionation occurs during halite formation (Vengosh et al., 1992; Liu et al., 2000). These fractionations and riverine input during basin isolation will drive the evaporite-hosted boron to low-$\delta^{11}B$ isotope values such that the fluid inclusion record likely provides a lower limit for the $\delta^{11}B_{sw}$ through time (i.e. $\delta^{11}B_{sw}$ is heavier than the halite fluid inclusions of Paris et al. (2010)). Nevertheless, evaporites form from modified seawater in isolated basins making them unlikely archives of representative ocean $\delta^{11}B$.

An alternative semi-empirical approach makes assumptions regarding the evolution of Cenozoic deep-ocean pH and a benthic $\delta^{11}B$ record to determine changes in $\delta^{11}B_{sw}$ (Fig. 2; Raitzsch and Hönisch, 2013). This method assumes (1) a near linear surface water pH increase of 0.39 over the past 50 Myrs (Berner and Kothavala, 2001; Tyrrell and Zeebe, 2004; Ridgwell, 2005), and (2) a constant surface to deep ocean pH gradient of 0.3 (Tyrrell and Zeebe, 2004, and modern observations). The modeled surface pH and estimated fixed pH gradient is then used to estimate deep ocean pH, which can be converted to $\delta^{11}B_{sw}$ based on benthic foraminiferal $\delta^{11}B$ measurements. While this approach yields a qualitative independent check on other approaches (e.g. halite inclusions, geochemical modeling), as a quantitative record of $\delta^{11}B_{sw}$ through time, it has a number of drawbacks. Firstly, some of the $CO_2$ data used in the modeling studies is derived using the boron isotope-pH proxy, leading to some circularity in the methodology. Secondly, given the structure in $CO_2$ proxy records, the assumption that surface ocean pH changed linearly through the Cenozoic is most likely an oversimplification (Beerling and Royer, 2011). Consequently, while this method may shed some light on the evolution of $\delta^{11}B_{sw}$ through time, it cannot be subsequently used to determine pH or atmospheric $CO_2$ from $\delta^{11}B$ of foraminiferal calcite because the $\delta^{11}B_{sw}$ record is itself based on assumptions of the secular evolution of pH and $CO_2$.

One of the big challenges of reconstructing a $\delta^{11}B_{sw}$ record empirically is determining $\delta^{11}B_{sw}$ without relying on dependent pH constraints. One way to avoid using absolute

Clim. Past Discuss., doi:10.5194/cp-2015-177, 2016
Manuscript under review for journal Clim. Past
Published: 26 January 2016


pH reconstructions is to exploit the non-linear relationship between $\delta^{11}B$ and pH alongside estimated pH gradients in the ocean to constrain $\delta^{11}B_{sw}$. The non-linear relationship between $\delta^{11}B$ and pH means that the pH difference between two $\delta^{11}B$ data points varies as a function of $\delta^{11}B_{sw}$ (Fig. 3). Consequently if the size of the pH gradient can be estimated, irrespective of absolute pH, then there is only one $\delta^{11}B_{sw}$ value that is consistent with the foraminiferal $\delta^{11}B$ measurements and the specified pH gradient (Fig. 3c).

Previously this approach has been applied to pH variations in the surface ocean and used in studies of Cenozoic $pCO_2$ to account for changes in $\delta^{11}B_{sw}$ (determined using $\delta^{11}B$ in surface and thermocline-dwelling foraminifera) (Fig. 2) (Palmer et al., 1998; Pearson and Palmer 1999, Pearson and Palmer 2000). This approach uses a constant pH gradient between the surface and some depth proximal to the oxygen minimum zone and the boron isotope values of a mixed layer dwelling species and thermocline dweller to calculate a value for $\delta^{11}B_{sw}$ (Pearson and Palmer, 1999). The resultant curve produced by this method shows that $\delta^{11}B_{sw}$ varies between 37.7‰ and 39.4‰ through the Neogene (Fig. 2) (Pearson and Palmer, 2000). Unfortunately, the applicability of this $\delta^{11}B_{sw}$ record (derived from $\delta^{11}B$ data measured using NTIMS) to $\delta^{11}B$ records generated using the MC-ICPMS is uncertain (Foster et al., 2013). In addition, this $\delta^{11}B_{sw}$ record is determined using a fractionation factor of 1.0194 (Kakihana et al., 1977), whereas recent experimental data have shown the value to be higher (1.0272 ± 0.0006, Klochko et al., 2006). Thirdly, given our understanding of the $\delta^{11}B$ difference between species/size fractions (Foster, 2008; Henehan et al., 2013), the mixed species and size fractions used to make the $\delta^{11}B$ measurements in that study may have introduced some additional uncertainty in the reconstructed $\delta^{11}B_{sw}$. Consequently, while the estimates from Pearson and Palmer (2000) show that the rationale behind this approach can yield useful $\delta^{11}B_{sw}$ estimates that may be qualitatively correct, the underlying measurements and some of the key assumptions have led to uncertainties in the record.

The same method, but using planktic-benthic instead of surface planktic- thermocline planktic $\delta^{11}B$ gradients to calculate $\delta^{11}B_{sw}$, was recently applied to the middle Miocene where it yielded a $\delta^{11}B_{sw}$ of $37.6\ ^{+0.4}_{-0.5}$ ‰ (Foster et al., 2012). The major limitation of these pH gradient approaches is the assumption of a constant pH

Clim. Past Discuss., doi:10.5194/cp-2015-177, 2016
Manuscript under review for journal Clim. Past
Published: 26 January 2016


gradient through time. A useful extension to this method therefore utilises the $\delta^{13}C$ in foraminiferal calcite to estimate the surface-to-deep pH gradient and then determine $\delta^{11}B_{sw}$ (Foster et al., 2012). Here we expand on the study of Foster et al. (2012) and present a number of new $\delta^{11}B_{sw}$ records based on $\delta^{11}B$ measured in planktic-benthic pairs. In our first treatment of the data we assume that the pH gradient has remained the same as modern at each site through time. In the second approach we utilise benthic-planktic $\delta^{13}C$ gradients to correct for changes in the pH gradient. Using a biogeochemical box model and an Earth system model we also assess the extent to which the relationship between pH and $\delta^{13}C$ gradients has remained constant under a comprehensive range of hypothetical carbon system and oceanographic states. We also use this model output to determine which pH/$\delta^{13}C$ regression is most appropriate for our data. In this study we focus on reconstructing $\delta^{11}B_{sw}$, whereas implications of our record in terms of the evolution of Neogene ocean pH and atmospheric $pCO_2$ are documented in a follow up study (Sosdian et al., *submitted*).

## 2. Methods

### 2.1 Site Locations and Age Models

Foraminifera from four sites are used to construct the planktic-benthic $\delta^{11}B$ pairs; Ocean Drilling Program, ODP, Site 758 and ODP Site 999 for the Pleistocene and Pliocene samples and ODP Site 926 and Site 761 for the Miocene (this study; Foster et al., 2012; Martinez-Boti et al., 2015a, Sosdian et al., *submitted*). We also incorporate the middle Miocene planktic-benthic pair from Site 761 in Foster et al., (2012). In order to put all the sites on a single age model at Site 999, Site 926 and Site 761 the biostratigraphy is used from (Shipboard Scientific Party, 1997), (Shipboard Scientific Party, 1995; Zeeden et al., 2013) and (Holbourn et al., 2004) respectively and updated to GTS2012 (Gradstein et al., 2012). At Site 758 the magnetostratigraphy (Shipboard Scientific Party, 1989) is used and updated to GTS2012 (Gradstein et al., 2012).

Clim. Past Discuss., doi:10.5194/cp-2015-177, 2016
Manuscript under review for journal Clim. Past
Published: 26 January 2016


Climate of the Past Discussions

## 2.2 Boron Isotope Analysis and pH Calculation

The boron isotope measurements (expressed in delta notation as $\delta^{11}B$ – permil variation) were made relative to the boric acid standard SRM 951; (Catanzaro et al., 1970). Boron was first separated from the Ca matrix prior to analysis using the boron specific resin Amberlite IRA 743 following Foster et al. (2013). The boron isotopic composition was then determined using a sample-standard bracketing routine on a ThermoFisher Scientific Neptune multicollector inductively coupled plasma mass spectrometer (MC-ICPMS) at the University of Southampton (following Foster et al., 2013). The relationship between $\delta^{11}B$ of $B(OH)_4^-$ and pH is very closely approximated by the following equation:

$$pH = pK_B^* - \log\left(-\frac{\delta^{11}B_{SW} - \delta^{11}B_{CaCO_3}}{\delta^{11}B_{SW} - \propto_B . \delta^{11}B_{CaCO_3} - 1000 . (\propto_B - 1)}\right) \qquad (1)$$

Where $pK_B^*$ is the equilibrium constant, dependent on salinity, temperature, pressure and seawater major ion composition (i.e., [Ca] and [Mg]), $\propto_B$ is the fractionation factor between the two boron species and $\delta^{11}B_{sw}$ is the boron isotope composition of seawater. Here we use a fractionation factor of 1.0272, calculated spectrophotometrically (Klochko et al., 2006). Although the $\delta^{11}B$ of foraminifera correlates well with pH and hence $[CO_2]_{aq}$, the $\delta^{11}B_{calcite}$ is often not exactly equal to $\delta^{11}B_{borate}$ (Sanyal et al., 2001; Foster, 2008; Henehan et al., 2013). The planktic species used to construct the benthic-planktic pairs changes through time, as a single species is not available for the entire Neogene (this study; Foster et al., 2012; Martìnez-Botì et al., 2015a, Sosdian et al., submitted). Here *Globigerinoides ruber* is used for 0 to 3 Ma, *Trilobatus sacculifer* (formally *Globigerinoides sacculifer* and including *Trilobatus trilobus*; Hembleden et al., 1987; Spezzaferri et al., 2015) for 0 to 20 Ma and *Globigerina praebulloides* for 22 to 23 Ma. The calibration for *G. ruber* (300-355µm) is from Henehan et al., (2013), *T. sacculifer* (300-355µm) from Sosdian et al., (*submitted*) where the *T. sacculifer* calibration of (Sanyal et al., 2001) is used with a modified intercept so that it passes through the core top value for *T. sacculifer* (300–355 µm) from ODP Hole 999A (Seki et al., 2010). Unlike the asymbiotic modern *T. bulloides, G. praebulloides* appears to be symbiotic at least in

Clim. Past Discuss., doi:10.5194/cp-2015-177, 2016
Manuscript under review for journal Clim. Past
Published: 26 January 2016


the latest Oligocene (Pearson and Wade, 2009). Therefore, we apply the *T. sacculifer* (300-355µm) calibration to this species. For *T. sacculifer* (500-600µm) at 0.7 Ma, we use the calibration from Martìnez-Botì et al., (2015b). In order to constrain deep-water pH, analysis was conducted on benthic foraminifera *Cibicidoides wuellestorfi* or *Cibicidoides mundulus* depending on which species were most abundant in each sample. The $\delta^{11}B$ of both *Cibicidoides* species shows no offset from the theoretical $\delta^{11}B$ of the borate ion and therefore no calibration is needed to adjust for species-specific offsets (Rae et al., 2011).

As mentioned above, in addition to $\delta^{11}B_{calcite}$, temperature, salinity, water depth (pressure) and seawater major ion composition are also needed to calculate pH from $\delta^{11}B$. We use the MyAMI specific ion interaction model (Hain et al., 2015) to calculate the appropriate equilibrium constants based on existing [Ca] and [Mg] reconstructions (Horita et al., 2002; Brennan et al., 2013). Sea surface temperature (SST) is calculated from tandem Mg/Ca analyses on planktic foraminifera (with a conservative 2σ uncertainty of 2°C). Adjustments were made for changes in $Mg/Ca_{sw}$ using the records of Horita et al. (2002) and Brennan et al. (2013), and correcting for changes in dependence on $Mg/Ca_{sw}$ following Evans and Muller (2012) using H = 0.41 calculated from *T. sacculifer* (Delaney et al., 1985; Hasiuk and Lohmann, 2010; Evans and Muller, 2012) using the equations:

$$Mg/Ca_{sw.c} = (Mg/Ca_{sw.a} \ / Mg/Ca_{sw.m})^{0.41} \qquad (2)$$

Where $Mg/Ca_{sw.c}$ is the correction factor applied to the temperature equation for changing $Mg/Ca_{sw}$, $Mg/Ca_{sw.a}$ is the estimated $Mg/Ca_{sw}$ for the age of the sample and $Mg/Ca_{sw.m}$ is modern $Mg/Ca_{sw}$. Temperature is then calculated using the generic planktic foraminifera calibration of Anand et al. (2003) and including a correction factor for $Mg/Ca_{sw}$.

$$Temperature = ln(Mg/Ca_{test}/(0.38 * Mg/Ca_{sw.c}))/0.09 \qquad (3)$$

Mg/Ca analysis was conducted on a small aliquot of the sample dissolved for isotope analysis at the University of Southampton using a ThermoFisher Scientific Element 2 XR. Al/Ca was also measured to assess the competency of the sample cleaning. Because of complications with the Mg/Ca-temperature proxy in *Cibicidoides* species (Elderfield et al., 2006), bottom water temperatures (BWTs) are estimated here by

Clim. Past Discuss., doi:10.5194/cp-2015-177, 2016
Manuscript under review for journal Clim. Past
Published: 26 January 2016


taking the global secular temperature change from the Mg/Ca temperature compilation of Cramer et al. (2011), using the calibration of Lear et al. (2010) and applying this change to the modern bottom water temperature at each site taken from the nearest GLODAP site (with a conservative 2σ uncertainty of 2ºC). Salinity is held constant at modern values determined from the nearest GLODAP site (2σ uncertainty of 2 ‰ uncertainty) for the entire record. Note that temperature and salinity have little influence on the calculated pH and the uncertainty in $\delta^{11}B_{sw}$ is dominated by the uncertainty in the $\delta^{11}B$ measurement and the estimate of the pH gradient.

The majority of the $\delta^{13}C$ data were measured at Cardiff University on a ThermoFinnigan MAT 252 coupled with a Kiel III carbonate device for automated sample preparation. Additional samples were measured on a gas source mass spectrometer Europa GEO 20-20, University of Southampton National Oceanography Centre Southampton (USNOCS) equipped with automated carbonate preparation device and on a Finnigan MAT 253 gas isotope ratio mass spectrometer connected to a Kiel IV automated carbonate preparation device at the Zentrum für Marine Tropenökologie (ZMT), Bremen. The Pliocene benthic $\delta^{13}C$ from Site 999 was taken from the nearest sample in Haug and Tiedemann, (1998). Stable isotope results are reported relative to the Vienna Peedee belemnite (VPDB) standard. An adjustment for vital effects on the $\delta^{13}C$ of *G. ruber* (+0.94 ‰; Spero et al., 2003), *T. sacculifer*/*G. praebulloides* (+0.46 ‰; Spero et al., 2003; Al-Rousan et al., 2004;), *C. mundulus* (+0.47 ‰; McCorkle et al., 1997) and *C. wuellestorfi* (+0.1 ‰; McCorkle et al., 1997) is applied to calculate the $\delta^{13}C$ of dissolved inorganic carbon (DIC).

### 2.3 Carbon isotopes as a proxy for vertical ocean pH gradient

The use of $\delta^{13}C$ in foraminiferal calcite to estimate the surface to deep pH gradient requires knowledge of the slope of the pH-$\delta^{13}C$ relationship in the past. In this section we briefly outlines the main factors that contribute to the pH-$\delta^{13}C$ relationship in order to underpin our analysis of extensive carbon cycle model simulations.

The production, sinking and sequestration into the ocean interior of low-$\delta^{13}C$ organic carbon via the soft-tissue component of the biological pump (e.g., Hain et al., 2014a) leads to broad correlation between $\delta^{13}C$, $[CO_3^{2-}]$ and macronutrients in the ocean. The remineralization of this organic matter decreases $\delta^{13}C$ and titrates $[CO_3^{2-}]$ so as to

Clim. Past Discuss., doi:10.5194/cp-2015-177, 2016
Manuscript under review for journal Clim. Past
Published: 26 January 2016


reduce pH, while nutrient concentrations are increased. In waters that have experienced more soft tissue remineralization both pH and $\delta^{13}C$ will be lower (Fig. 4a,b), which is the dominant cause for the positive slope between $\delta^{13}C$ and pH in the modern ocean (e.g., Foster et al., 2012; Fig. 4c).

Another significant factor affecting the spatial distribution of both $\delta^{13}C$ and pH is seawater temperature, which affects both the equilibrium solubility of DIC and the equilibrium isotopic composition of DIC. Warmer ocean waters have decreased equilibrium solubility of DIC and so increased local [$CO_3^{2-}$] and pH (Goodwin and Lauderdale, 2013), while warmer waters have relatively low equilibrium $\delta^{13}C$ values (Lynch-Stieglitz et al, 1995). This means that a spatial gradient in temperature acts to drive $\delta^{13}C$ and pH in opposite directions: warmer waters tend to have higher pH but lower $\delta^{13}C$. These opposing temperature effects act to reduce the pH difference between two points with greatly different temperature to below the value expected based on $\delta^{13}C$ alone. That is, when using $\delta^{13}C$ differences to estimate the pH gradient between the warm low latitude surface and cold deep waters the appropriate pH-$\delta^{13}C$ relationship will be less than expected when only considering the effect of the biological pump.

In the modern ocean, and for the preceding tens of millions of years, these two processes are likely dominant in setting spatial variation in $\delta^{13}C$ and pH (and [$CO_3^{2-}$]). However, other processes will have a minor effect on either pH or $\delta^{13}C$. For instance, the accumulation of remineralized $CaCO_3$ hard-tissue increases [$CO_3^{2-}$] and pH (Broecker and Peng, 1982), but does not significantly affect $\delta^{13}C$ (Zeebe and Wolf-Gladrow, 2001). Moreover, the long timescale of air/sea isotopic equilibration of $CO_2$ is an important factor in setting the distribution of $\delta^{13}C$ on a global ocean scale (Galbraith et al., 2015). The surface $CO_2$ disequilibrium also has a substantial effect on $\delta^{13}C$ (Lynch-Stieglitz et al., 1995) while it affects [$CO_3^{2-}$] and pH only marginally (Goodwin and Lauderdale, 2013).

Clim. Past Discuss., doi:10.5194/cp-2015-177, 2016
Manuscript under review for journal Clim. Past
Published: 26 January 2016


Climate of the Past Discussions

### 2.4 Modelling the pH to $\delta^{13}C$ relationship

After correcting for the Suess effect, modern ocean observations demonstrate a near linear relationship between global ocean data of seawater *in situ* pH and $\delta^{13}C$ DIC with a slope of 0.201 (Foster et al., 2012). This empirically determined slope might well have been different in past oceans with very different carbon chemistry compared to today. Here we use an ensemble approach with two independent carbon cycle models to show that the pH to $\delta^{13}C$ slope can only have changed in very tight limits. Below we provide pertinent information on the GENIE and CYCLOPS model experiments:

We use the Earth System model GENIE-1 (Edwards and Marsh, 2005; Ridgwell et al. 2007) to assess the robustness of the pH-$\delta^{13}C$ relationship and its sensitivity to physical and biogeochemical ocean forcing. The configuration used here is closely related to that of Holden et al. (2013), in which the controls on the ocean's $\delta^{13}C$ distribution were assessed, with an energy and moisture balance in the atmosphere, simple representations of land vegetation and sea ice, and frictional geostrophic ocean physics. In each of 16 vertical levels in the ocean, increasing in thickness with depth, there are 36x36 grid cells (10° in longitude and nominally 5° in latitude, with higher resolution at low latitudes). Modern ocean bathymetry and land topography is applied in all simulations. The ocean biogeochemical scheme (Ridgwell et al. 2007) is based on conversion of DIC to organic carbon associated with phosphate uptake with fixed P:C:O stoichiometry. Organic carbon and nutrients are remineralized according to a remineralization profile with a pre-defined *e*-folding depth scale. This depth scale, as well as the rain ratio of inorganic to organic carbon in sinking particulate matter, is among the parameters examined in the sensitivity study. In these simulations, there is no interaction with sediments. As a result of this, a steady state solution is obtained within the 5000-year simulations; the results presented here are for the end of the simulations.

The sensitivity study consists of seven sets of experiments, each varying a single model parameter relative to the control simulation with preindustrial atmospheric $pCO_2$. This enables us to assess both which processes, if any, are capable of altering the ocean's pH-$\delta^{13}C$ relationship, and the uncertainty in the predictive skill of this relationship due to spatial variability. These experiments are therefore exploratory in

Clim. Past Discuss., doi:10.5194/cp-2015-177, 2016
Manuscript under review for journal Clim. Past
Published: 26 January 2016


nature and not intended to represent real changes that may have occurred. The seven parameters varied are (1) the ocean's alkalinity reservoir; (2) the ocean's carbon reservoir; (3) the parameter "S. Lim gas exchange" which blocks air-sea gas exchange south of the stated latitude, significant here because of the dependence of $\delta^{13}C$ on surface disequilibrium (Galbraith et al., 2015); (4) inorganic to organic carbon rain ratio, controlling the relationship between DIC and alkalinity distributions; (5) "Antarctic shelf FWF", a freshwater flux adjustment (always switched off in control experiments with GENIE) facilitating the formation of brine rich waters, which produces a high-salinity poorly-ventilated deep ocean at high values; (6) "Atlantic-Pacific FWF", a freshwater flux adjustment equivalent to freshwater hosing, leading to a shut-down of the Atlantic meridional overturning circulation at low values; (7) remineralization depth-scale of sinking organic matter, which affects the vertical gradient both of pH and $\delta^{13}C$. A wide range of parameter values is chosen for each parameter in order to exceed any plausible changes within the Cenozoic.

For the second test of the slope of pH-$\delta^{13}C$ relationship we use the CYCLOPS biogeochemical 18-box model that includes a dynamical lysocline, a subantarctic zone surface box and a polar Antarctic zone box (Sigman et al., 1998; Hain et al., 2010, 2014b). The very large model ensemble with 13,500 individual model scenarios is designed to capture the full plausible range of (a) glacial/interglacial carbon cycle states by sampling the full solution space of Hain et al. (2010), and (b) reconstructed secular changes in seawater [Ca] (calcium concentration), carbonate compensation depth (CCD), weathering and atmospheric $CO_2$. The following seven model parameters are systematically sampled to set the 13,500 model scenarios: (1) shallow versus deep Atlantic meridional overturning circulation represented by modern reference north Atlantic deep water (NADW) versus peak glacial North Atlantic intermediate water (GNAIW) circulation; (2) iron driven changes in nutrient drawdown in the subantarctic zone of the Southern Ocean; (3) changes in nutrient drawdown of the polar Antarctic; (4) changes in vertical exchange between the deep Southern Ocean and the polar Antarctic surface; (5) range in seawater [Ca] concentration from 1x to 1.5x modern as per reconstructions (Horita et al., 2002); (6) Pacific CCD is set to the range of 4.4-4.9 km via changes in the weathering flux, as per sedimentological evidence (Pälike et al., 2012); (7) atmospheric $CO_2$ is set from

Clim. Past Discuss., doi:10.5194/cp-2015-177, 2016
Manuscript under review for journal Clim. Past
Published: 26 January 2016


200 ppm to 1000 ppm by changes in the 'weatherability' parameter of the silicate weathering mechanism. The ensemble spans predicted bulk ocean DIC between 1500 and 4500 $\mu$mol/kg, a wide range of ocean pH and $CaCO_3$ saturation states consistent with the open system weathering cycle, and widely different states of the ocean's biological pump.

### 2.5 Assessing uncertainty

$\delta^{11}B_{sw}$ uncertainty was calculated using a Monte Carlo approach where pH was calculated for deep and surface waters at each time slice using a random sampling (n=10000) of the various input parameters within their respective uncertainties as represented by normal distributions. These uncertainties (2σ uncertainty in parentheses) are: temperature (± 2 °C), salinity (±2 units on the practical salinity scale) [Ca] (± 4.5 mmol/kg), [Mg], (± 4.5 mmol/kg), $\delta^{11}B_{planktic}$ (± 0.15-0.42 ‰), $\delta^{11}B_{benthic}$ (± 0.21-0.61 ‰), and either the fixed modern pH gradient at that site (± 0.05 pH units) or the pH gradient predicted by the $\delta^{13}C$-pH relationship (± 0.05 pH units). In our first approach we assume the pH gradient at each site has remained the same as modern through time (gradient estimated from GLODAP; Key et al., 2004). In the second approach the pH gradient is corrected using the $\delta^{13}C$ gradient (where the slope of the relationship between pH and $\delta^{13}C$ is taken from the CYCLOPS model). The uncertainty in the $\delta^{11}B$ measurements is calculated from the long-term reproducibility of Japanese Geological Survey *Porites* coral standard (JCP; $\delta^{11}B$=24.3‰) at the University of Southampton using the equations:

$$2\sigma = 2.25\,\exp^{-23.01[^{11}B]} + 0.28\,\exp^{-0.64[^{11}B]} \quad (4)$$

$$2\sigma = 33450\,\exp^{-168.2[^{11}B]} + 0.311\,\exp^{-1.477[^{11}B]} \quad (5)$$

where $[^{11}B]$ is the intensity of $^{11}B$ signal in volts and equation (4) and equation (5) used with $10^{11}$ Ω and $10^{12}$ Ω resistors, respectively.

From the 10,000 Monte Carlo ensemble solutions of our 22 benthic-planktic pairs we construct 10,000 randomized records of $\delta^{11}B_{sw}$ as a function of time. Each of these randomized $\delta^{11}B_{sw}$ records is subjected to smoothing using the locally weighted scatterplot smoothing (LOWESS) algorithm with a smoothing parameter (span) of 0.7, which prevents the smoothed $\delta^{11}B_{sw}$ from changing faster than allowed by

Clim. Past Discuss., doi:10.5194/cp-2015-177, 2016
Manuscript under review for journal Clim. Past
Published: 26 January 2016


seawater boron mass balance (~0.1 ‰ per million years; boron residence time is 11-17 million years; Lemarchand et al., 2002). As a result of anomalously low $\delta^{11}B$ differences between benthic and planktic pairs, two pairs at 8.68 Ma and 19 Ma were discarded from the smoothing. The spread of the ensemble of smoothed $\delta^{11}B_{sw}$ curves represents the combination of the compounded, propagated uncertainties of the various inputs and the additional constraint of gradual $\delta^{11}B_{sw}$ change over geological time. Various statistical properties (i.e., mean, median, standard deviation (σ), various quantiles) of this $\delta^{11}B_{sw}$ reconstruction were evaluated from the ensemble of smoothed $\delta^{11}B_{sw}$ records. Generally, for any given benthic-planktic pair the resulting $\delta^{11}B_{sw}$ estimates are not perfectly normally distributed and thus we use the median as the metric for the central tendency.

## 3. Results and Discussion

### 3.1 $\delta^{11}B$ benthic and planktic data

Surface and deep-ocean, $\delta^{11}B$, $\delta^{13}C$ and temperature broadly show a similar pattern to one another throughout the Neogene (Fig. 5). The $\delta^{11}B$ benthic record decreases from ~15 ‰ at 24 Ma to a minimum of 13.28 ‰ at 14 Ma before increasing to ~17 ‰ at present day (Fig. 5). This pattern and the range of values in benthic foraminiferal $\delta^{11}B$ is in keeping with previously published Neogene $\delta^{11}B$ benthic records measured using NTIMS (Raitzsch and Hönisch, 2013), suggesting that our deep-water $\delta^{11}B$ record is representative of large scale pH changes in the global ocean. While the surface $\delta^{11}B_{borate}$ remained relatively constant between 24 and 11 Ma at ~ 16 ‰, there is a significant increase in $\delta^{11}B$ between the middle Miocene and present (values increase to ~ 20 ‰) (Fig. 5b). The reconstructed surface water temperatures show a long-term decrease through the Neogene from ~ 28°C to 24°C, aside from during the Miocene Climatic Optimum (MCO) where maximum Neogene temperatures are reached (Fig. 5c). Following Cramer et al. (2011) deep-water temperatures decrease from ~ 12°C to 4°C at the present day and similarly show maximum temperatures in the MCO. Surface and deep-water $\delta^{13}C_{DIC}$ both broadly decrease through the Neogene and appear to covary on shorter timescales (Fig. 5e, f).

Clim. Past Discuss., doi:10.5194/cp-2015-177, 2016
Manuscript under review for journal Clim. Past
Published: 26 January 2016


Climate of the Past Discussions

### 3.2 The relationship between $\delta^{13}C$ and pH gradients

In the global modern ocean data, after accounting for the anthropogenic carbon, the empirical relationship between *in situ* pH and DIC $\delta^{13}C$ is well described by a linear function with a slope of 0.201 (Fig. 4; Foster et al., 2012). In the control GENIE experiment and in all experiments in which ocean-physics parameters (Antarctic shelf FWF and Atlantic-Pacific FWF) are varied, the pH/$\delta^{13}C$ gradient is slightly greater than 0.2, with a root-mean-squared error (RMSE) of ~0.05 in a reconstruction of the spatial distribution of pH using this relationship (Fig. 6). Varying the biogeochemical parameters (gas exchange, rain ratio and remineralizing depth scale) yields some change in the regressed slope of the pH/$\delta^{13}C$ relationship due to decoupled responses of pH and $\delta^{13}C$, but this gradient remains well within the 0.2 +/- 0.05 range, and a RMSE of 0.05 in the spatial relationship remains robust (Fig. 6). We take this as evidence that the uncertainty in the pH/$\delta^{13}C$ relationship assumed in our carbon chemistry calculation is well represented by a central value of 0.2 with a 0.025 standard deviation. Experiments at very high DIC or low alkalinity, either of which yield high atmospheric $pCO_2$ and low mean ocean pH, yield gradients slightly outside the 0.2 +/- 0.05 range, with an elevated RMSE. This is probably associated with the non-linearity of the pH scale, modifying the gradient for a very different pH. It is to be emphasised that such extreme decoupled changes in DIC and alkalinity are not plausible within the Cenozoic, and were only possible in these simulations because of the absence of interactive sediments.

The slope of the pH-$\delta^{13}C$ relationship simulated by our CYCLOPS model ensemble across a range of perturbed states is 0.2047 ($1\sigma = 0.0196$) (Fig. 7a, 8), in perfect agreement with modern empirical data and our GENIE experiments. We take this agreement as evidence that the slope of the pH-$\delta^{13}C$ relationship is a feature of ocean biogeochemistry that is relatively conserved even if ocean carbon chemistry and circulation change drastically. For the purpose of calculating $\delta^{11}B_{sw}$ from our benthic/planktic foraminfera measurements we need to estimate the pH difference between the low latitude surface and deep ocean at the sample sites, most of which are in the subtropical North Atlantic. If we restrict our analysis of the CYCLOPS ensemble to only the low latitude surface boxes and the corresponding deep ocean boxes (i.e., Atlantic, Indian, South Pacific and North Pacific) the slope of the

Clim. Past Discuss., doi:10.5194/cp-2015-177, 2016
Manuscript under review for journal Clim. Past
Published: 26 January 2016


applicable pH-$\delta^{13}C$ relationship is 0.1797 (1σ = 0.0213) (Fig. 7b, 8), which is significantly less than the regression based on all 18 model boxes. Further, if only the Atlantic low latitude surface and deep ocean boxes are used to calculate the slope of the applicable pH- $\delta^{13}C$ relationship declines to 0.1655 (1σ = 0.0192) (Fig. 7c, 8). Thus, excluding the polar ocean and the ocean's mid-depth permanent thermocline from the analysis consistently yields a shallower slope of the pH-$\delta^{13}C$ relationship, with some evidence for water mass dependence also in the modern observations (Fig. 4). Here we calculate $\delta^{11}B_{sw}$ for all three estimates of the pH- $\delta^{13}C$ slope (global regression 0.201; low latitude surface and deep regression 0.1797; Atlantic low latitude surface to deep box gradients 0.1655) assuming a generous uncertainty of 0.05 (2 σ) in all cases, and we provide all three $\delta^{11}B_{sw}$ scenarios as an online supplement. Overall, the slope between pH and $\delta^{13}C$ is dependent on the competition between spatial variations in remineralized soft tissue, increasing the slope between pH and $\delta^{13}C$, and seawater temperature, decreasing the slope between pH and $\delta^{13}C$. The largest concentrations of remineralized soft tissue occur in the thermocline, suggesting that a relatively steep pH-$\delta^{13}C$ slope is appropriate for estimating the pH gradient from the $\delta^{13}C$ difference. However, when comparing surface to deep waters, as is done in this study, the full range of the temperature effect is expressed and a relatively shallow pH-$\delta^{13}C$ slope is appropriate. This is particularly true given that our samples are from the low latitude surface and the cold deep ocean. Since most of our measurements are from the subtropical Atlantic it is perhaps most appropriate to use the slope regressed from the low latitude surface and deep boxes from this ocean basin (i.e., $\Delta pH/\Delta \delta^{13}C = 0.1655$; with 1σ = 0.025) and we will focus on those calculations in the following discussion (Fig. 9).

### 3.3 $\delta^{11}B_{sw}$ records through the Neogene

The individual $\delta^{11}B_{sw}$ estimates calculated using the modern pH gradient method vary from 34.9 ‰ to 42.2 ‰ (± 0.84-4.77 ‰) across the Neogene with a predominance of higher values closer to the modern and lowest values in the middle Miocene (Fig. 9). After smoothing is applied to satisfy seawater B mass balance, the long-term $\delta^{11}B_{sw}$ is determined as 37.5 ‰ at 23 Ma, decreases to a minimum of 37.17 ‰ at ~ 13 Ma (± 0.34-1.81 ‰), and subsequently increases gradually towards modern values through the late Miocene, Pliocene and Pleistocene (Fig. 9). The variability in the estimations

Clim. Past Discuss., doi:10.5194/cp-2015-177, 2016
Manuscript under review for journal Clim. Past
Published: 26 January 2016


of $\delta^{11}B_{sw}$ for each individual benthic/planktic foraminifera pair suggest that individual estimates of $\delta^{11}B_{sw}$ are sensitive to the different input parameters, particularly the assigned uncertainty in the pH gradient. However, by smoothing the record we effectively suppress error that is uncorrelated between individual benthic/planktic pairs of similar age and thereby focus on the effect of changes in $\delta^{11}B_{sw}$ that are correlated over multi-million year timescales.

When using $\delta^{13}C$ gradients as predictors for the pH gradient the $\delta^{11}B_{sw}$ values calculated are broadly similar to the results with assumed constant pH gradient: $\delta^{11}B_{sw}$ varies from 34.1 ‰ to 42.3 ‰ (± 0.72-4.0 ‰) across the Neogene with the predominance of higher values closer to the modern with the lowest values in the middle Miocene (Fig. 9). However, when the individual $\delta^{11}B_{sw}$ estimates are smoothed, while the $\delta^{11}B_{sw}$ calculated using this method is similar to the constant pH gradient scenario through the late and middle Miocene (~ 37.5 ‰ ± 0.19-1.28 ‰), the subsequent increase occurs more rapidly and the $\delta^{11}B_{sw}$ record reaches modern values by ~5 Ma (Fig. 9). Given the variability we observe in the $\delta^{13}C$ derived pH gradient, and the consistency between the modelled pH gradient using GENIE and CYCLOPS, we conclude using the benthic-to-planktic pH difference calculated using the $\delta^{13}C$ gradient is indeed an improvement over the assumption that pH gradients remained constant through time. Therefore, we recommend the use of the $\delta^{13}C$-corrected $\delta^{11}B_{sw}$ moving forward and in the following discussion we will limit our attention to this record.

### 3.4 Comparison to other $\delta^{11}B_{sw}$ records

The comparison of our new $\delta^{11}B_{sw}$ record to those previously published, reveals that a common feature of all the existing estimates of Neogene $\delta^{11}B_{sw}$ evolution is an increase through time from the middle Miocene to present (Fig. 10). Our new $\delta^{11}B_{sw}$ record is broadly similar to previously published estimates calculated using pH gradients in the surface ocean, in terms of both shape of the record and magnitude of the reconstructed changes, with the notable exception in the early and middle Miocene where $\delta^{11}B_{sw}$ in our record is 0.5 ‰ lower (Fig. 10) than the published estimates of Pearson and Palmer (2000). The $\delta^{11}B_{sw}$ record calculated using benthic $\delta^{11}B$ and assumed deep ocean pH changes (Raitzsch and Hönisch, 2013) is also rather

Clim. Past Discuss., doi:10.5194/cp-2015-177, 2016
Manuscript under review for journal Clim. Past
Published: 26 January 2016


similar to the $\delta^{11}B_{sw}$ values reconstructed here, with 9 out of 16 of their individual samples falling inside our 95% confidence band even before considering the large individual sample uncertainties reported by Raitzsch and Hönisch (2013). That said, the polynomial fit to the data applied by Raitzsch and Hönisch (2013) takes no account of the uncertainties of individual data points and produces an oscillating pattern that is inconsistent with our new reconstruction (Fig. 10). Furthermore, our new $\delta^{11}B_{sw}$ record falls within the broad uncertainty envelope of boron mass balance calculations of Lemarchand et al. (2002), but those modelled values do not show the same level of multi-million year variability of either Raitzsch and Hönisch (2013) or our new record, therefore suggesting that some of the controls on ocean inputs and outputs of boron are not fully understood. In line with the conclusions of previous studies (e.g., Raitzsch and Hönisch, 2013), our data show that the $\delta^{11}B_{sw}$ signal in the fluid inclusions (Paris et al., 2010) is mostly likely a combination of the $\delta^{11}B_{sw}$ and some other factor such as a poorly constrained fractionation factor between the seawater and the halite.

### 3.5 Common controls on the seawater isotopic ratios of B, Mg, Ca and Li

Our new record of $\delta^{11}B_{sw}$ has some similarities to secular change seen in other marine stable isotope records (Fig. 11). The $\delta^{7}Li_{sw}$ (Misra and Froelich, 2012) and $\delta^{44/40}Ca_{sw}$ (Griffith et al., 2008) both increase through the Neogene, whereas $\delta^{26}Mg_{sw}$ decreases (Pogge von Strandmann et al., 2014) suggesting a similar control on the isotopic composition of all four elements across this time interval (Fig. 11). To further evaluate the correlation between these other marine isotope records and $\delta^{11}B_{sw}$, we interpolate and cross-plot $\delta^{11}B_{sw}$ and the $\delta^{7}Li_{sw}$, $\delta^{44/40}Ca_{sw}$ and $\delta^{26}Mg_{sw}$ records. This analysis suggests that the isotopic composition of $\delta^{11}B_{sw}$, $\delta^{7}Li_{sw}$, $\delta^{26}Mg_{sw}$ and $\delta^{44/40}Ca_{sw}$ are well correlated through the Neogene, although there is some scatter in these relationships (Fig. 12). Although the Sr isotope record shows a similar increase during the Neogene (Hodell et al., 1991), we elect to focus our discussion on $\delta^{11}B_{sw}$, $\delta^{7}Li_{sw}$, $\delta^{26}Mg_{sw}$ and $\delta^{44/40}Ca_{sw}$ given that the factors fractionating these isotope systems are similar (see below).

To better constrain the controls on $\delta^{11}B_{sw}$, $\delta^{7}Li_{sw}$, $\delta^{26}Mg_{sw}$ and $\delta^{44/40}Ca_{sw}$ it is instructive to compare the size and isotopic composition of the fluxes of boron,

Clim. Past Discuss., doi:10.5194/cp-2015-177, 2016
Manuscript under review for journal Clim. Past
Published: 26 January 2016


lithium, calcium and magnesium (Table 1). As noted previously, the major flux of boron into the ocean is via riverine input (Lemarchand et al., 2002), although some studies suggest that atmospheric input may also play an important role (Park and Schlesinger, 2002). The outputs are dominated by adsorption onto clays and the alteration of oceanic crust (Spivack and Edmond, 1987; Smith et al., 1995). Similar to boron the primary inputs of lithium into the ocean come from hydrothermal sources and riverine input and the main outputs are ocean crust alteration and adsorption onto sediments (Misra and Froelich, 2012). The two dominant controls on magnesium concentration and isotope ratio in the oceans is the riverine input, ocean crust alteration and dolomitization (Table 1) (Tipper et al., 2006b). The main controls on the amount of calcium in the modern ocean and its isotopic composition is the balance between riverine and hydrothermal inputs and removal through $CaCO_3$ deposition and alteration of oceanic crust (Fantle and Tipper, 2014, Griffith et al., 2008). Dolomitization has also been cited as playing a potential role in controlling $\delta^{44/40}Ca_{sw}$, although the contribution of this process through time is poorly constrained (Griffith et al., 2008).

Analysis of the oceanic fluxes of all four ions suggests that riverine input may be an important factor influencing the changing isotopic composition of B, Li, Ca and Mg over the late Neogene (Table 1). In the case of all four elements, a combination of the isotopic ratio of the source rock and isotopic fractionation during weathering processes are typically used to explain the isotopic composition of a particular river system. However, in most cases the isotopic composition of the source rock is found to be of secondary importance (Rose et al., 2000; Kısakűrek et al., 2005; Tipper et al., 2006b; Millot et al., 2010). For instance, the $\delta^{11}B$ composition of rivers is primarily dependent on isotopic fractionation during the reaction of water with silicate rocks and to a lesser extent the isotopic composition of the source rock (i.e. the proportion of evaporites and silicate rocks; Rose et al., 2000). The source rock also appears to have limited influence on the $\delta^{7}Li$ composition of rivers and riverine $\delta^{7}Li$ varies primarily with weathering intensity (Kısakűrek et al., 2005; Millot et al., 2010). The riverine input of calcium to the oceans is controlled by the composition of the primary continental crust (dominated by carbonate weathering) and a recycled component, although the relative influence of these two processes is not well understood (Tipper et al., 2006a). In addition, vegetation may also play a significant

Clim. Past Discuss., doi:10.5194/cp-2015-177, 2016
Manuscript under review for journal Clim. Past
Published: 26 January 2016


role in the $\delta^{44/40}$Ca of rivers (Fantle and Tipper, 2014). For Mg, the isotopic composition of the source rock is important for small rivers, however, lithology is of limited significance at a global scale in comparison to fractionation in the weathering environment (Tipper et al., 2006b). Given the lack of evidence of source rock as a dominant control on the isotopic composition of rivers, here we focus on some of the possible causes for changes in the isotopic composition and/or flux of riverine input over the Neogene.

In this regard, of the four elements discussed here, the Li isotopic system is the most extensively studied. Indeed, the change in $\delta^7Li_{sw}$ has already been attributed to an increase in the $\delta^7Li_{sw}$ composition of the riverine input (Hathorne and James, 2006; Misra and Froelich, 2012). The causes of the shift in $\delta^7$Li riverine have been variably attributed to: (1) an increase in incongruent weathering of silicate rocks and secondary clay formation as a consequence of Himalayan uplift (Misra and Froelich, 2012), (2) a reduction in weathering intensity (Hathorne and James, 2006; Froelich and Misra, 2014), (3) an increase in silicate weathering rate (Liu et al., 2015) and 4) an increase in the formation of floodplains and the increased formation of secondary minerals (Pogge von Strandmann and Henderson, 2014). In all four cases the lighter isotope of Li is retained on land in clay and secondary minerals. A mechanism associated with either an increase in secondary mineral formation or the retention of these minerals on land is also consistent across Mg, Ca and B isotope systems. For instance, clay minerals are preferentially enriched in the light isotope of B (Spivack and Edmond, 1987; Deyhle and Kopf, 2004; Lemarchand and Gaillardet, 2006) and Li (Pistiner and Henderson, 2003) and soil carbonates and clays are preferentially enriched in the light isotope of Ca (Tipper et al., 2006a; Hindshaw et al., 2013; Ockert et al., 2013). The formation of secondary silicate minerals, such as clays, is assumed to preferentially take up heavy Mg isotope into the solid phase (Tipper et al., 2006a; Tipper et al., 2006b; Pogge von Strandmann et al., 2008; Wimpenny et al., 2014), adequately explaining the inverse relationship between $\delta^{11}B_{sw}$ and $\delta^{26}Mg_{sw}$. Consequently the increased formation or retention on land of secondary minerals would alter the isotopic composition of the riverine input of all the examined isotope systems and could potentially explain the trends in all four isotope systems through the late Neogene (Fig. 12). The increased formation and retention of clays on land may have been related to the growth of the Himalayan orogeny and increased clay

Clim. Past Discuss., doi:10.5194/cp-2015-177, 2016
Manuscript under review for journal Clim. Past
Published: 26 January 2016


formation in the newly formed floodplains and foreland surrounding the mountains (Pogge von Strandmann and Henderson, 2014).

## 4 Conclusions

Here we present a new $\delta^{11}B_{sw}$ record for the Neogene based on paired planktic-benthic $\delta^{11}B$ measurements. Our new record suggests that $\delta^{11}B_{sw}$ is ~ 37.5 ‰ at the Oligocene-Miocene boundary and remains low through the middle Miocene. $\delta^{11}B_{sw}$ then increases to the modern value through the late Miocene. This new $\delta^{11}B_{sw}$ record provides a vital constraint required to estimate Neogene ocean pH, ocean carbon chemistry and atmospheric $CO_2$ using the $\delta^{11}B$-pH proxy. When the new $\delta^{11}B_{sw}$ record is compared to changes in the seawater isotopic composition of Li, Ca and Mg the shape of the records across the Neogene is remarkably similar. In all four cases riverine input is cited as one of the key control of the isotopic composition of the elements in seawater. When we compare the isotopic fractionation of the elements associated with secondary mineral formation, the trends in the $\delta^{26}Mg_{sw}$, $\delta^{44/40}Ca_{sw}$ $\delta^{11}B_{sw}$ and $\delta^{7}Li_{sw}$ records are all consistent with an increase in secondary mineral formation through time. While a more quantitative treatment of these multiple stable isotope systems is required, the $\delta^{11}B_{sw}$ record presented here provides additional constraints on the processes responsible for the evolution of ocean chemistry through time.

**Acknowledgements:**

This work used samples provided by (I)ODP, which is sponsored by the U.S. National Science Foundation and participating countries under the management of Joint Oceanographic Institutions, Inc. We thank W. Hale and A. Wuelbers of the Bremen Core Repository for their kind assistance. The work was supported by NERC grants NE/I006176/1 (G.L.F. and C.H.L.), NE/H006273/1 (G.L.F), NE/I006168/1 and NE/K014137/1 (P.A.W), a NERC Independent Research Fellowship NE/K00901X/1 (M.P.H.) and a NERC studentship (R.G). Matthew Cooper, J. Andy Milton, and the B-team are acknowledged for their assistance in the laboratory.

**References:**

Al-Rousan, S., Pätzold, J., Al-Moghrabi, S., and Wefer, G., 2004, Invasion of anthropogenic $CO_2$ recorded in planktonic foraminifera from the northern Gulf of Aqaba: International Journal of Earth Sciences, v. 93, no. 6, p. 1066-1076.

Anand, P., Elderfield, H., and Conte, M. H., 2003, Calibration of Mg/Ca thermometry in planktonic foraminifera from a sediment trap time series: Paleoceanography, v. 18, no. 2, DOI: 10.1029/2002PA000846.

Bartoli, G., Hönisch, B., Zeebe, R.E., 2011, Atmospheric $CO_2$ decline during the Pliocene intensification of Northern Hemisphere glaciations: Paleoceanography, v.26, DOI: 10.1029/2010PA002055.

Badger, M. P. S., Lear, C.H., Pancost, R.D., Foster, G.L., Bailey, T.R., Leng, M.J., and Abels, H.A., 2013, $CO_2$ drawdown following the middle Miocene expansion of the Antarctic Ice Sheet: Paleoceanography, v. 28, doi:10.1002/palo.20015.

Beerling, D. J., and Royer, D. L., 2011, Convergent Cenozoic $CO_2$ history: Nature Geosci, v. 4, no. 7, p. 418-420.

Berner, R. A., and Kothavala, Z., 2001, GEOCARB III: A revised model of atmospheric $CO_2$ over Phanerozoic time: American Journal of Science, v. 301, no. 2, p. 182-204.

Brennan S. T., Lowenstein T. K., Cendón D. I., 2013, The major-ion composition of Cenozoic seawater: the past 36 million years from fluid inclusions in marine halite: American Journal of Science, v. 313, p. 713–775.

Broecker, W. S. and T. H. Peng, 1982, Tracers in the Sea, Lamont-Doherty Earth Observatory, Palisades, N. Y.

Burton, K.W., Vigier, N., 2012, Lithium isotopes as tracers in Marine and terrestrial environments, Handbook of Environmental Isotope Geochemistry, Springer, Berlin, Heidelberg, p. 41–59.

CARINA Group, 2009, Carbon in the Atlantic Ocean Region - the CARINA project: Results and Data, Version 1.0: Carbon Dioxide Information Analysis Center, Oak Ridge National Laboratory, U.S. Department of Energy, Oak Ridge, Tennessee. doi: 10.3334/CDIAC/otg.CARINA.ATL.V1.0

Catanzaro, E. J., Champion, C., Garner, E., Marinenko, G., Sappenfield, K., and W., S., 1970, Boric Acid: Isotopic and Assay Standard Reference Materials NBS (US) Special Publications. National Bureau of Standards, Institute for Materials Research, Washington, DC.

Cramer, B., Miller, K., Barrett, P., and Wright, J., 2011, Late Cretaceous-Neogene trends in deep ocean temperature and continental ice volume: Reconciling records of benthic foraminiferal geochemistry ($\delta^{18}O$ and Mg/Ca) with sea level history: Journal of Geophysical Research-Oceans, v. 116, doi:10.1029/2011JC007255.

Delaney, M. L., Be, A. W. H., and Boyle, E. A., 1985, Li, Sr, Mg and Na in foraminiferal calcite shells from laboratory culture, sediment traps and sediment cores: Geochimica Et Cosmochimica Acta, v. 49, no. 6, p. 1327-1341.

Deyhle, A., and Kopf, A., 2004, Possible influence of clay contamination on B isotope geochemistry of carbonaceous samples: Applied Geochemistry, v. 19, no. 5, p. 737-745.

Edwards, N. R. and Marsh, R., 2005, Uncertainties due to transport- parameter sensitivity in an efficient 3-D ocean-climate model: Clim. Dynam., 24, 415–433, doi:10.1007/s00382-004-0508-8.

Elderfield, H., Yu, J., Anand, P., Kiefer, T., and Nyland, B., 2006, Calibrations for benthic foraminiferal Mg/Ca paleothermometry and the carbonate ion hypothesis: Earth and Planetary Science Letters, v. 250, no. 3-4, p. 633-649.

Evans, D., and Muller, W., 2012, Deep time foraminifera Mg/Ca paleothermometry: Nonlinear correction for secular change in seawater Mg/Ca: Paleoceanography, v. 27, DOI: 10.1029/2012PA002315.

Fantle, M.S., Tipper, E.T, 2014, Calcium isotopes in the global biogeochemical Ca cycle: Implications for development of a Ca isotope proxy, Earth-Science Reviews, v. 129, p. 148-177.

Foster, G., Hönisch, B., Paris, G., Dwyer, G., Rae, J., Elliott, T., Gaillardet, J., Hemming, N., Louvat, P., and Vengosh, A., 2013, Interlaboratory comparison of boron isotope analyses of boric acid, seawater and marine $CaCO_3$ by MC-ICPMS and NTIMS: Chemical Geology, v. 358, p. 1-14.

Foster, G., Lear, C. H., and Rae, J.W.B., 2012, The evolution of $pCO_2$, ice volume and climate during the middle Miocene: Earth and Planetary Science Letters, v. 341-344, p. 243-254.

Foster, G. L., 2008, Seawater pH, $pCO_2$ and [$CO_3^{2-}$] variations in the Caribbean Sea over the last 130 kyr: A boron isotope and B/Ca study of planktic forminifera: Earth and Planetary Science Letters, v. 271, no. 1-4, p. 254-266.

Foster, G. L., Pogge von Strandmann, P. A. E., and Rae, J. W. B., 2010, Boron and magnesium isotopic composition of seawater: Geochemistry Geophysics Geosystems, v. 11, DOI: 10.1029/2010GC003201.

Froelich, F., and Misra, S., 2014. Was the late Paleocene-early Eocene hot because Earth was flat? An ocean lithium isotope view of mountain building, continental weathering, carbon dioxide, and Earth's Cenozoic climate: Oceanography, v. 27, no.1, p. 36–49.

Galbraith, E.D., Kwon, E.Y., Bianchi, D., Hain, M.P., Sarmiento, J.L., 2015, The impact of atmospheric $pCO_2$ on carbon isotope ratios of the atmosphere and ocean: Global Biogeochemical Cycles, 9, 307–324, doi:10.1002/2014GB004929

Goodwin, P., and J. M. Lauderdale 2013, Carbonate ion concentrations, ocean carbon storage, and atmospheric $CO_2$: Global Biogeochem. Cycles, 27, doi:10.1002/gbc.20078.

Gradstein F.M., Ogg J.G., Schmitz M., Ogg G., 2012, The Geologic Time Scale 2012: Boston, Elsevier, 1144 p., doi:10.1016/B978-0-444-59425-9.00004-4.

Greenop, R., Foster, G. L., Wilson, P. A., and Lear, C. H., 2014, Middle Miocene climate instability associated with high-amplitude $CO_2$ variability: Paleoceanography, v. 29, no. 9, DOI: 2014PA002653.

Griffith, E., Paytan, A., Caldeira, K., Bullen, T., and Thomas, E., 2008, A Dynamic Marine Calcium Cycle During the Past 28 Million Years: Science, v. 322, no. 5908, p. 1671-1674.

Hain, M.P., Sigman, D.M., and Haug, G.H., 2010, Carbon dioxide effects of Antarctic stratification, North Atlantic Intermediate Water formation, and subantarctic nutrient drawdown during the last ice age: Diagnosis and

synthesis in a geochemical box model: Global Biogeochem. Cycles, v. 24, doi:10.1029/2010GB003790.

Hain, M.P, Sigman, D.M., and Haug, G.H., 2014a, The Biological Pump in the Past, Treatise on Geochemistry 2nd ed., vol. 8, chapter 18, 485-517, doi:10.1016/B978-0-08-095975-7.00618-5

Hain, M.P, Sigman, D.M., and Haug, G.H., 2014b, Distinct roles of the Southern Ocean and North Atlantic in the deglacial atmospheric radiocarbon decline: Earth and Planetary Science Letters, v.394, p.198-208, doi: 10.1016/j.epsl.2014.03.020

Hain, M.P, Sigman, D.M., Higgins, J.A., and Haug, G.H., 2015, The effects of secular calcium and magnesium concentration changes on the thermodynamics of seawater acid/base chemistry: Implications for Eocene and Cretaceous ocean carbon chemistry and buffering: Global Biogeochem. Cycles, v. 29, doi:10.1002/2014GB004986.

Hasiuk, F., and Lohmann, K., 2010, Application of calcite Mg partitioning functions to the reconstruction of paleocean Mg/Ca: Geochimica Et Cosmochimica Acta, v. 74, no. 23, p. 6751-6763.

Hathorne, E. C., and James, R. H., 2006, Temporal record of lithium in seawater: A tracer for silicate weathering?: Earth and Planetary Science Letters, v. 246, no. 3–4, p. 393-406.

Haug, G. H., and Tiedemann, R., 1998, Effect of the formation of the Isthmus of Panama on Atlantic Ocean thermohaline circulation: Nature, v. 393, no. 6686, p. 673-676.

Hemleben Ch, Spindler M, Breitinger, Ott R., 1987, Morphological and physiological responses of *Globigerinoides sacculifer* (Brady) under varying laboratory conditions: Marine Micropaleontology, v.12, p. 305-324.

Hemming, N. G., and Hanson, G. N., 1992, Boron isotopic composition and concentration in modern marine carbonates: Geochimica et Cosmochimica Acta, v. 56, no. 1, p. 537-543.

Henehan, M. J., Rae, J. W. B., Foster, G. L., Erez, J., Prentice, K. C., Kucera, M., Bostock, H. C., Martìnez-Botì, M. A., Milton, J. A., Wilson, P. A., Marshall, B. J., and Elliott, T., 2013, Calibration of the boron isotope proxy in the planktonic foraminifera Globigerinoides ruber for use in palaeo-$CO_2$ reconstruction: Earth and Planetary Science Letters, v. 364, no. 0, p. 111-122.

Hindshaw, R. S., Bourdon, B., Pogge von Strandmann, P. A. E., Vigier, N., and Burton, K. W., 2013, The stable calcium isotopic composition of rivers draining basaltic catchments in Iceland: Earth and Planetary Science Letters, v. 374, no. 0, p. 173-184.

Hodell, D.A., Mueller, P.A., Garrido, J.R., 1991, Variations in the strontium isotopic composition of seawater during the Neogene: Geology, v.11, p. 24-27.

Holbourn, A., Kuhnt, W., Simo, J., and Li, Q., 2004, Middle Miocene isotope stratigraphy and paleoceanographic evolution of the northwest and southwest Australian margins (Wombat Plateau and Great Australian Bight): Palaeogeography Palaeoclimatology Palaeoecology, v. 208, no. 1-2, p. 1-22.

Holden, P. B., N. R. Edwards, S. A. Müller, K. I. C. Oliver, R. M. De'ath and A. Ridgwell, 2013. Controls on the spatial distribution of oceanic $\delta^{13}C_{DIC}$: Biogeosciences 10, 1815-1833.

Hönisch, B., Hemming, N. G., Archer, D., Siddall, M., and McManus, J. F., 2009, Atmospheric Carbon Dioxide Concentration Across the Mid-Pleistocene Transition: Science, v. 324, no. 5934, p. 1551-1554.

Horita, J., Zimmermann, H., and Holland, H. D., 2002, Chemical evolution of seawater during the Phanerozoic: Implications from the record of marine evaporites: Geochimica Et Cosmochimica Acta, v. 66, no. 21, p. 3733-3756.

Kakihana, H., Kotaka, M., Satoh, S., Nomura, M., and Okamoto, M., 1977, Fundamental studies on ion-exchange separation of boron isotopes: Bulletin of the Chemical Society of Japan, v. 50, no. 1, p. 158-163.

Key, R. M., Kozyr, A., Sabine, C. L., Lee, K., Wanninkhof, R., Bullister, J. L., Feely, R. A., Millero, F. J., Mordy, C., and Peng, T. H., 2004, A global ocean carbon climatology: Results from Global Data Analysis Project (GLODAP): Global Biogeochem. Cycles, v. 18, no. 4, doi:10.1029/2004GB002247.

Kısakűrek, B., James, R. H., and Harris, N. B. W., 2005, Li and $\delta^7$Li in Himalayan rivers: Proxies for silicate weathering?: Earth and Planetary Science Letters, v. 237, no. 3–4, p. 387-401.

Klochko, K., Kaufman, A. J., Yao, W. S., Byrne, R. H., and Tossell, J. A., 2006, Experimental measurement of boron isotope fractionation in seawater: Earth and Planetary Science Letters, v. 248, no. 1-2, p. 276-285.

Lear, C. H., Mawbey, E. M., and Rosenthal, Y., 2010, Cenozoic benthic foraminiferal Mg/Ca and Li/Ca records: Toward unlocking temperatures and saturation states: Paleoceanography, v. 25, doi:10.1029/2009PA001880.

Lee, K., Kim, T. W., Byrne, R. H., Millero, F. J., Feely, R. A., and Liu, Y. M., 2010, The universal ratio of boron to chlorinity for the North Pacific and North Atlantic oceans: Geochimica Et Cosmochimica Acta, v. 74, no. 6, p. 1801-1811.

Lemarchand, D., and Gaillardet, J., 2006, Transient features of the erosion of shales in the Mackenzie basin (Canada), evidences from boron isotopes: Earth and Planetary Science Letters, v. 245, no. 1–2, p. 174-189.

Lemarchand, D., Gaillardet, J., Lewin, E., and Allegre, C. J., 2002, Boron isotope systematics in large rivers: implications for the marine boron budget and paleo-pH reconstruction over the Cenozoic: Chemical Geology, v. 190, no. 1-4, p. 123-140.

Liu, W. G., Xiao, Y. K., Peng, Z. C., An, Z. S., and He, X. X., 2000, Boron concentration and isotopic composition of halite from experiments and salt lakes in the Qaidam Basin: Geochimica Et Cosmochimica Acta, v. 64, no. 13, p. 2177-2183.

Liu, X.-M., Wanner, C., Rudnick, R. L., and McDonough, W. F., 2015, Processes controlling $\delta^7$Li in rivers illuminated by study of streams and groundwaters draining basalts: Earth and Planetary Science Letters, v. 409, no. 0, p. 212-224.

Lynch-Steiglitz, J., T.F. Stocker, W.S. Broecker and R.G. Fairbanks (1995), The influence of air-sea exchange on the isotopic composition of oceanic carbon: Observations and modeling: Global Biogeochemical Cycles, vol. 9, 4, p653-665.

Martìnez-Botì, M. A., Foster, G. L., Chalk, T. B., Rohling, E. J., Sexton, P. F., Lunt, D. J., Pancost, R. D., Badger, M. P. S., and Schmidt, D. N., 2015a, Plio-Pleistocene climate sensitivity from on a new high-resolution $CO_2$ record: Nature, v. 518, p. 49-54.

Martìnez-Botì, M.A., Marino, G., Foster, G. L., Ziveri, P., Henehan, M. J., Rae, J. W. B., Mortyn, P. G. and Vance, D., 2015b, Boron isotope evidence for oceanic $CO_2$ leakage during the last deglaciation: Nature, v. 518, p. 219-222.

McCorkle, D. C., Corliss, B. H., and Farnham, C. A., 1997, Vertical distributions and stable isotopic compositions of live (stained) benthic foraminifera from the North Carolina and California continental margins: Deep Sea Research Part I: Oceanographic Research Papers, v. 44, no. 6, p. 983-1024.

Millot, R., Vigier, N., and Gaillardet, J., 2010, Behaviour of lithium and its isotopes during weathering in the Mackenzie Basin, Canada: Geochimica et Cosmochimica Acta, v. 74, no. 14, p. 3897-3912.

Misra, S., and Froelich, P., 2012, Lithium Isotope History of Cenozoic Seawater: Changes in Silicate Weathering and Reverse Weathering: Science, v. 335, no. 6070, p. 818-823.

Ockert, C., Gussone, N., Kaufhold, S., Teichert, B.M.A., 2013, Isotope fractionation during Ca exchange on clay minerals in a marine environment: Geochimica et Cosmochimica Acta, v. 112, p. 374-388.

Olsen, A., Ninneman, U.S., 2010, Large $\delta^{13}C$ gradients in the preindustrial North Atlantic revealed: Science, v. 330, p. 658–659.

Pälike, H., Lyle, M., Nishi, H., Raffi, I., Ridgwell, A., Gamage, K., Klaus, A., Acton, G., Anderson, L., Backman, J., Baldauf, J., Beltran, C., *et al.* 2012, A Cenozoic record of the equatorial Pacific carbonate compensation depth: Nature, v. 488, no. 7413, p. 609-614.

Palmer, M. R., Pearson, P. N., and Cobb, S. J., 1998, Reconstructing past ocean pH-depth profiles: Science, v. 282, no. 5393, p. 1468-1471.

Paris, G., Gaillardet, J., and Louvat, P., 2010, Geological evolution of seawater boron isotopic composition recorded in evaporites: Geology, v. 38, no. 11, p. 1035-1038.

Park, H., and Schlesinger, W. H., 2002, Global biogeochemical cycle of boron: Global Biogeochemical Cycles, v. 16, no. 4, DOI: 10.1029/2001GB001766.

Pearson, P. N., Foster, G. L., and Wade, B. S., 2009, Atmospheric carbon dioxide through the Eocene-Oligocene climate transition: Nature, v. 461, p. 1110-1113.

Pearson, P. N., and Wade, B. S., 2009, Taxonomy and Stable Isotope Paleoecology of Well-Preserved Planktonic Foraminifera from the Uppermost Oligocene of Trinidad: Journal of Foraminiferal Research, v. 39, no. 3, p. 191-217.

Pearson, P. N., and Palmer, M. R., 1999, Middle Eocene seawater pH and atmospheric carbon dioxide concentrations: Science, v. 284, no. 5421, p. 1824-1826.

Pearson, P. N., and Palmer, M. R., 2000, Atmospheric carbon dioxide concentrations over the past 60 million years: Nature, v. 406, no. 6797, p. 695-699.

Pistiner, J. S., and Henderson, G. M., 2003, Lithium-isotope fractionation during continental weathering processes: Earth and Planetary Science Letters, v. 214, no. 1–2, p. 327-339.

Pogge von Strandmann, P. A. E., Burton, K. W., James, R. H., van Calsteren, P., Gislason, S. R., and Sigfússon, B., 2008, The influence of weathering processes on riverine magnesium isotopes in a basaltic terrain: Earth and Planetary Science Letters, v. 276, no. 1–2, p. 187-197.

Pogge von Strandmann, P. A. E., Forshaw, J., and Schmidt, D. N., 2014, Modern and Cenozoic records of seawater magnesium from foraminiferal Mg isotopes: Biogeosciences, v. 11, no. 18, p. 5155-5168.

Pogge von Strandmann, P. A. E., and Henderson, G. M., 2014, The Li isotope response to mountain uplift: Geology, doi: 10.1130/G36162.1.

Rae, J. W. B., Foster, G. L., Schmidt, D. N., and Elliott, T., 2011, Boron isotopes and B/Ca in benthic foraminifera: Proxies for the deep ocean carbonate system: Earth and Planetary Science Letters, v. 302, no. 3-4, p. 403-413.

Raitzsch, M., and Hönisch, B., 2013, Cenozoic boron isotope variations in benthic foraminifers: Geology, v. 41, no. 5, p. 591-594.

Ridgewell, A., 2005, A mid Mesozoic revolution in the regulation of ocean chemistry: Marine Geology, v. 217, no. 3-4, p. 339-357.

Ridgwell, A., Hargreaves, J. C., Edwards, N. R., Annan, J. D., Lenton, T. M., Marsh, R., Yool, A., and Watson, A., 2007, Marine geo-chemical data assimilation in an efficient Earth System Model of global biogeochemical cycling: Biogeosciences, 4, 87–104, doi:10.5194/bg-4-87-2007, 2007.

Rose, E. F., Chaussidon, M., and France-Lanord, C., 2000, Fractionation of boron isotopes during erosion processes: the example of Himalayan rivers: Geochimica et Cosmochimica Acta, v. 64, no. 3, p. 397-408.

Rose-Koga, E. F., Sheppard, S. M. F., Chaussidon, M., and Carignan, J., 2006, Boron isotopic composition of atmospheric precipitations and liquid–vapour fractionations: Geochimica et Cosmochimica Acta, v. 70, no. 7, p. 1603-1615.

Sanyal, A., Bijma, J., Spero, H., and Lea, D. W., 2001, Empirical relationship between pH and the boron isotopic composition of Globigerinoides sacculifer: Implications for the boron isotope paleo-pH proxy: Paleoceanography, v. 16, no. 5, p. 515-519.

Schlitzer, R., Ocean Data View, 2010, http://www.awi-bremerhaven.de/GEO/ODV.

Seki, O., Foster, G. L., Schmidt, D. N., Mackensen, A., Kawamura, K., and Pancost, R. D., 2010, Alkenone and boron-based Pliocene $pCO_2$ records: Earth and Planetary Science Letters, v. 292, no. 1-2, p. 201-211.

Shipboard Scientific Party, 1989. Site 758. *In* Peirce, J., Weissel, J., et al., *Proc. ODP, Init. Repts.*, 121: College Station, TX (Ocean Drilling Program), 359–453. doi:10.2973/odp.proc.ir.121.112.1989

Shipboard Scientific Party, 1995. Site 926. *In* Curry, W.B., Shackleton, N.J., Richter, C., et al., *Proc. ODP, Init. Repts.*, 154: College Station, TX (Ocean Drilling Program), 153–232. doi:10.2973/odp.proc.ir.154.105.1995

Shipboard Scientific Party, 1997. Site 999. *In* Sigurdsson, H., Leckie, R.M., Acton, G.D., et al., *Proc. ODP, Init. Repts.*, 165: College Station, TX (Ocean Drilling Program), 131–230. doi:10.2973/odp.proc.ir.165.104.1997.

Sigman, D.M., McCorkle, D.C., Martin, W.R., 1998, The calcite lysocline as a constraint on glacial/interglacial low-latitude production changes: Global Biogeochem. Cycles, v. 12, no. 3, p. 409-427.

Simon, L., Lecuyer, C., Marechal, C., and Coltice, N., 2006, Modelling the geochemical cycle of boron: Implications for the long-term $\delta^{11}B$ evolution of seawater and oceanic crust: Chemical Geology, v. 225, no. 1-2, p. 61-76.

Smith, H. J., Spivack, A. J., Staudigel, H., and Hart, S. R., 1995, The boron isotopic composition of altered oceanic crust: Chemical Geology, v. 126, no. 2, p. 119-135.

Sosdian, S.M., Greenop. R., Lear, C.H., Foster, G.L., Hain, M.P, and Pearson, P.N., 2015, Future ocean acidification could be unprecedented in the last 14 million years: submitted to Nature.

Spero, H., Mielke, K., Kalve, E., Lea, D., and Pak, D., 2003, Multispecies approach to reconstructing eastern equatorial Pacific thermocline hydrography during the past 360 kyr: Paleoceanography, v. 18, no. 1, doi:10.1029/2001GC000200.

Spezzaferri S, Kucera M, Pearson PN, Wade BS, Rappo S, Poole CR, et al., 2015, Fossil and genetic evidence for the polyphyletic nature of the planktonic foraminifera "*Globigerinoides*", and description of the new Genus *Trilobatus*: PLoS ONE, v.10, no. 5, DOI:e0128108. doi:10.1371/journal.pone.0128108

Spivack, A. J., and Edmond, J. M., 1987, Boron isotope exchange between seawater and the oceanic crust: Geochimica et Cosmochimica Acta, v. 51, no. 5, p. 1033-1043.

Tipper, E. T., Galy, A., and Bickle, M. J., 2006a, Riverine evidence for a fractionated reservoir of Ca and Mg on the continents: Implications for the oceanic Ca cycle: Earth and Planetary Science Letters, v. 247, no. 3–4, p. 267-279.

Tipper, E. T., Galy, A., Gaillardet, J., Bickle, M. J., Elderfield, H., and Carder, E. A., 2006b, The magnesium isotope budget of the modern ocean: Constraints from riverine magnesium isotope ratios: Earth and Planetary Science Letters, v. 250, no. 1–2, p. 241-253.

Tomascak, P. B., 2004, Developments in the Understanding and Application of Lithium Isotopes in the Earth and Planetary Sciences: Reviews in Mineralogy and Geochemistry, v. 55, no. 1, p. 153-195.

Tyrrell, T., and Zeebe, R. E., 2004, History of carbonate ion concentration over the last 100 million years: Geochimica Et Cosmochimica Acta, v. 68, no. 17, p. 3521-3530.

Vengosh, A., Starinsky, A., Kolodny, Y., Chivas, A. R., and Raab, M., 1992, Boron Isotope Variations during Fractional Evaporation of Sea-Water - New Constraints on the Marine Vs Nonmarine Debate: Geology, v. 20, no. 9, p. 799-802.

Wimpenny, J., Colla, C. A., Yin, Q.-Z., Rustad, J. R., and Casey, W. H., 2014, Investigating the behaviour of Mg isotopes during the formation of clay minerals: Geochimica et Cosmochimica Acta, v. 128, no. 0, p. 178-194.

Wombacher, F., Eisenhauer, A., Böhm, F., Gussone, N., Regenberg, M., Dullo, W. C., and Rüggeberg, A., 2011, Magnesium stable isotope fractionation in marine biogenic calcite and aragonite: Geochimica et Cosmochimica Acta, v. 75, no. 19, p. 5797-5818.

You, C.F., Spivack, A. J., Smith, J. H., and Gieskes, J. M., 1993, Mobilization of boron in convergent margins: Implications for the boron geochemical cycle: Geology, v. 21, no. 3, p. 207-210.

Zeebe, R. E., and Wolf-Gladrow, D. A., 2001, $CO_2$ in seawater, equilibrium, kinetics, isotopes IN Elsevier oceanography series, Amsterdam, PAYS-BAS, Elsevier, XIII, 346 p. p.:

Zeeden, C., Hilgen, F., Westerhold, T., Lourens, L., Röhl, U., and Bickert, T., 2013, Revised Miocene splice, astronomical tuning and calcareous plankton biochronology of ODP Site 926 between 5 and 14.4 Ma: Palaeogeography, Palaeoclimatology, Palaeoecology, v. 369, no. 0, p. 430-451.

**Figure Captions:**

Clim. Past Discuss., doi:10.5194/cp-2015-177, 2016
Manuscript under review for journal Clim. Past
Published: 26 January 2016


Figure 1: The oceanic boron cycle. Fluxes are from Lemarchand et al. (2002) and Park and Schlesinger (2002). Isotopic compositions are from Lemarchand et al. (2002) and references therein.

Figure 2: A compilation of published $\delta^{11}B_{sw}$ records. Seawater composition reconstructed from foraminifera depth profiles (light blue squares and dark blue cross) from Pearson and Palmer (2000) and Foster et al. (2012) respectively, numerical modelling (dark green line), with additional green lines shows ± 1 ‰ confidence interval (Lemarchand et al., 2002), benthic $\delta^{11}B$ (purple diamonds and line) from Raitzsch and Hönisch (2013), and halites (orange crosses) from Paris et al. (2010). All the published $\delta^{11}B_{sw}$ curves are adjusted so that at t=0, the isotopic composition is equal to the modern (39.61 ‰).

Figure 3: Schematic diagram showing the change in pH gradient with a 3‰ change in $\delta^{11}B$ for $\delta^{11}B_{sw}$ of a) 39.6‰ and b) 37.5‰. Note how a $\delta^{11}B$ difference of 3 ‰ is translated into different pH gradients depending on the $\delta^{11}B_{sw}$. Calculated using $B_T$= 432.6 μmol/kg (Lee et al., 2010) and $\alpha_B$= 1.0272 (Klochko et al., 2006). (c) The pH change for a $\delta^{11}B$ change of 3 ‰ at a range of different $\delta^{11}B_{sw}$.

Figure 4: Latitudinal cross-section through the Atlantic showing (a) pH variations; (b) the $\delta^{13}C$ composition. Data are plotted using Ocean Data View (Schlitzer 2001). pH data are from the CARINA dataset (CARINA group, 2009) and the $\delta^{13}C$ data are from the GLODAP data compilation (Key et al., 2004); (c) pH and $\delta^{13}C_{DIC}$ relationships in the modern ocean adapted from Foster et al., (2012). Because of anthropogenic acidification and the Seuss effect only data from >1500 m are plotted. Also included in the plot are the data from a transect in the North Atlantic (from 0 to 5000 m) where the effects of anthropogenic perturbation on both parameters have been corrected (Olsen and Ninneman, 2010).

Figure 5: $\delta^{11}B_{borate}$, temperature and $\delta^{13}C_{DIC}$ estimates for the surface and deep ocean through the last 23 million years. (a) $\delta^{11}B_{borate}$ surface; (b) $\delta^{11}B_{borate}$ deep (blue) from this study and (green) Raitzsch and Hönisch, (2013). The error bars show the analytical external reproducibility at 95% confidence; (c) Mg/Ca based temperature reconstructions calculated on paired measurements of surface dwelling planktic foraminifera; (d) Deep water temperature estimates from Cramer et al. (2011); (e)

Clim. Past Discuss., doi:10.5194/cp-2015-177, 2016
Manuscript under review for journal Clim. Past
Published: 26 January 2016


$\delta^{13}C_{DIC}$ surface record; (f) $\delta^{13}C_{DIC}$ benthic record. Squares depict ODP Site 999, triangles are ODP Site 758, diamonds are ODP Site 926, circles are ODP Site 761.

Figure 6: The output from sensitivity analysis of the relationship between pH gradient and $\delta^{13}C$ gradient from GENIE. The gradient of a linear regression for each experiment, with $\delta^{13}C$ and pH data taken from each grid square, is plotted. A pre-industrial model setup was taken and perturbations were made to alkalinity inventory, carbon inventory, Antarctic shelf fresh water flux (Sv), Atlantic-Pacific freshwater flux, S. Lim gas exchange (blocks air-sea gas exchange south of the stated latitude), remineralisation depth scale (m) and rain ratio – as described in the methods section. Blue circles depict the gradient (where the colour reflect the $CO_2$ level of each experiment) and red open circles show the root mean square of the regression (RMSE). The green data points (closed) are the gradient of the linear regression for the control experiment conducted at 292.67 ppm $CO_2$. The green (open) points show the RMSE for this control run. Inventories are dimensionless (1 is control). For the Atlantic-Pacific FWF 1 is equivalent to 0.32 Sv. The alkalinity and carbon inventory experiments are very extreme and inconsistent with geologic evidence. All other sensitivity test indicate a possible range from 0.195 to 0.205 for the slope of the pH/$\delta^{13}C$ regression.

Figure 7: The output from sensitivity analysis of the relationship between pH gradient and $\delta^{13}C$ gradient from the 13700 run CYCLOPS ensemble (see text for model details). Panel (a) shows the mean gradient when the result from all 18 ocean boxes are included in the regression. Panel (b) shows only the boxes from the low latitude ocean from all basins and (c) shows the regression from only North Atlantic low latitude boxes. Note the lower $\Delta pH/\Delta\delta^{11}B$ slope at the lower latitudes due to the effect of temperature.

Figure 8: The pH gradient between surface and deep through time calculated from the $\delta^{13}C$ gradient and using the whole ocean (blue) (panel (a) Fig. 7), low latitude (green) (panel (b) Fig. 7) and low latitude North Atlantic only (red) (panel (c) Fig. 7) based regressions from the CYCLOPS model.

Figure 9: The calculated $\delta^{11}B_{sw}$ from the benthic-planktic $\delta^{11}B$ pairs assuming (a) a pH gradient derived from (a) the modern pH (blue); (b) $\delta^{13}C$ (red). The uncertainty on each data point is determined using a Monte Carlo approach including

Clim. Past Discuss., doi:10.5194/cp-2015-177, 2016
Manuscript under review for journal Clim. Past
Published: 26 January 2016


uncertainties in temperature, salinity, $\delta^{11}B$ and the pH gradient (see text for details) The line of best fit is the probability maximum of a LOWESS fit given the uncertainty in the calculated $\delta^{11}B_{sw}$. The darker shaded area highlights the 68% confidence interval and the lighter interval highlights the 95% confidence interval. The circles highlight the data points that were removed prior to LOWESS smoothing; (c) shows an expanded view of the smoothed curves for ease of comparison between the variable pH gradient from $\delta^{13}C$ (red) and modern pH gradient (blue).

Figure 10: a) The $\delta^{11}B_{sw}$ curve calculated using the variable pH gradient derived from $\delta^{13}C$. The median (red line), 68% (dark red band) and 95% (light red band) confidence intervals are plotted. Plotted with a compilation of published $\delta^{11}B_{sw}$ records. Seawater composition reconstructed from foraminifera depth profiles (light blue squares and dark blue cross) from Pearson and Palmer (2000) and Foster et al. (2012) respectively, numerical modelling (dark green line), with additional green green lines shows ± 1 ‰ confidence interval (Lemarchand et al., 2002) and benthic $\delta^{11}B$ (purple diamonds and line) from Raitzsch and Hönisch (2013). All the published $\delta^{11}B_{sw}$ curves are adjusted so that at t=0, the isotopic composition is equal to the modern (39.61 ‰).

Figure 11: a) The $\delta^{11}B_{sw}$ curve calculated using the variable pH gradient derived from $\delta^{13}C$ (the darker shaded area highlights the 68% confidence interval and the lighter interval highlights the 95% confidence interval), $\delta^{26}Mg_{sw}$ record from Pogge von Strandmann et al. (2014) (error bars are ± 0.28 ‰ and include analytical uncertainty and scatter due to the spread in modern *O. universa* and the offset between the two analysed species), $\delta^{44/40}Ca_{sw}$ record from Griffith et al. (2008) (error bars show 2 σ uncertainty) and $\delta^{7}Li_{sw}$ record from Misra and Froelich (2012) (error bars show 2 σ uncertainty).

Figure 12: Crossplots of the records of $\delta^{11}B_{sw}$ using the variable pH gradient derived from $\delta^{13}C$ (error bars show 2 σ uncertainty) with $\delta^{44/40}Ca_{sw}$ from Griffith et al. (2008) (error bars show 2 σ uncertainty), $\delta^{7}Li_{sw}$ from Misra and Froelich (2012) (error bars show 2 σ uncertainty) and $\delta^{26}Mg_{sw}$ from Pogge von Strandmann et al. (2014) (error bars are ± 0.28 ‰ and include analytical uncertainty and scatter due to the spread in modern *O. universa* and the offset between the two analysed species). The colour of

Clim. Past Discuss., doi:10.5194/cp-2015-177, 2016
Manuscript under review for journal Clim. Past
Published: 26 January 2016


the data points highlights the age of the data points where red = modern and blue = 23 Ma.

Table 1: The average $\delta^{11}B$, $\delta^{26}Mg$, $\delta^{44/40}Ca$ and $\delta^{7}Li$ composition of major fluxes into and out of the ocean. Colour coding reflects the relative importance of each the processes (darker shading reflects greater importance). The colour coding for boron is based on Lemarchand et al. (2002) and references therein, lithium from Misra and Froelich (2012) and references therein, magnesium from Tipper et al. (2006b) and calcium from Fantle and Tipper (2014) and Griffin et al. (2008) and references therein. The isotopic ratio of each process is: (a) Lemarchand et al. (2002) and references therein; b) Misra and Froelich (2012) and references therein; (c) Burton and Vigier (2012); (d) Tipper et al. (2006b); e) Wombacher et al. (2011); f) includes dolomitisation; g) removal through hydrothermal activity; h) Griffith et al. (2008); i) Fantle and Tipper (2014) and references therein; j) dolomitisation may be an important component of the carbonate flux. Modern $\delta^{26}Mg_{sw}$ and $\delta^{11}B_{sw}$ from Foster et al. (2010), $\delta^{7}Li_{sw}$ from Tomascak (2004). The $\delta^{44/40}Ca$ presented here was measured relative to seawater and hence seawater has a $\delta^{44/40}Ca_{sw}$ of 0 permil by definition.

Clim. Past Discuss., doi:10.5194/cp-2015-177, 2016
Manuscript under review for journal Clim. Past
Published: 26 January 2016


Climate of the Past
Discussions
Open Access
EGU

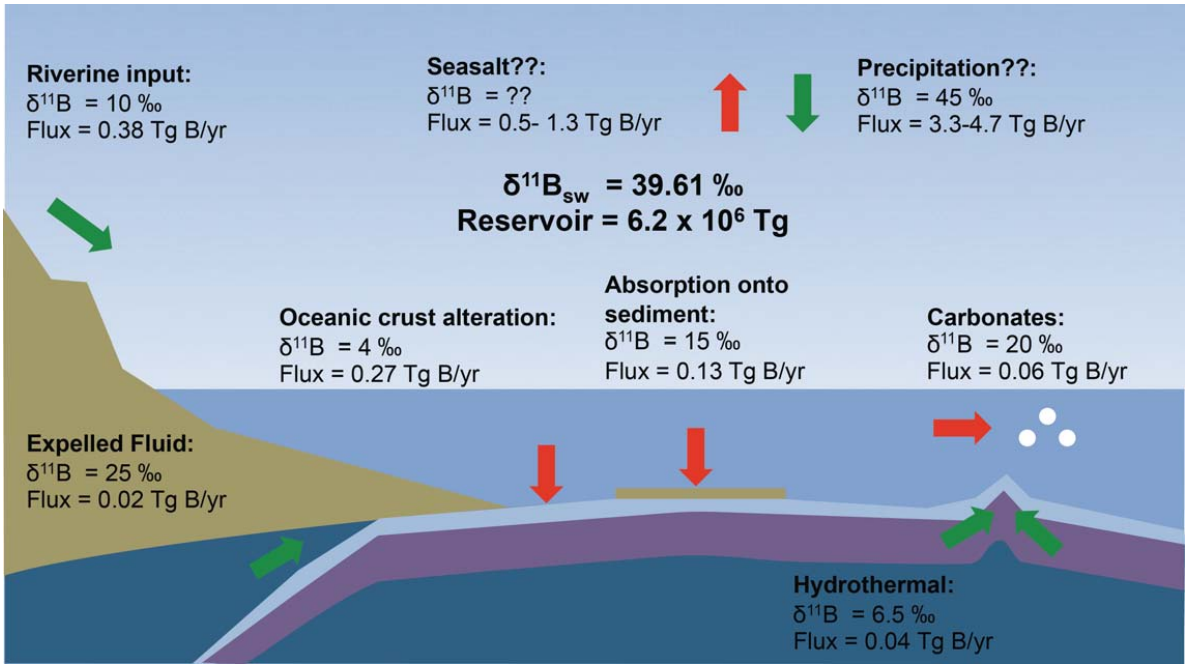

Clim. Past Discuss., doi:10.5194/cp-2015-177, 2016
Manuscript under review for journal Clim. Past
Published: 26 January 2016


Climate of the Past
Discussions
Open Access
EGU

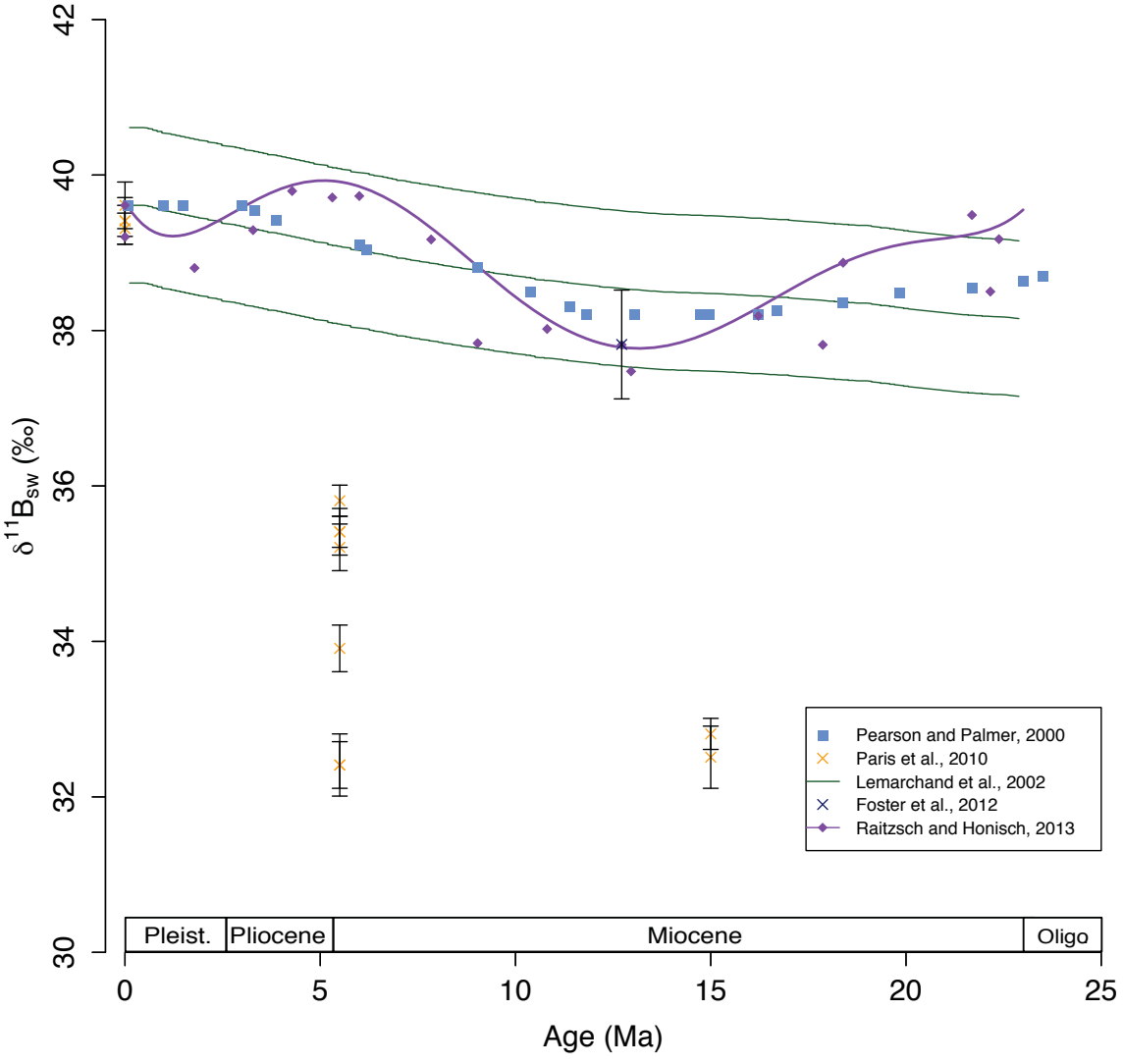

Clim. Past Discuss., doi:10.5194/cp-2015-177, 2016
Manuscript under review for journal Clim. Past
Published: 26 January 2016


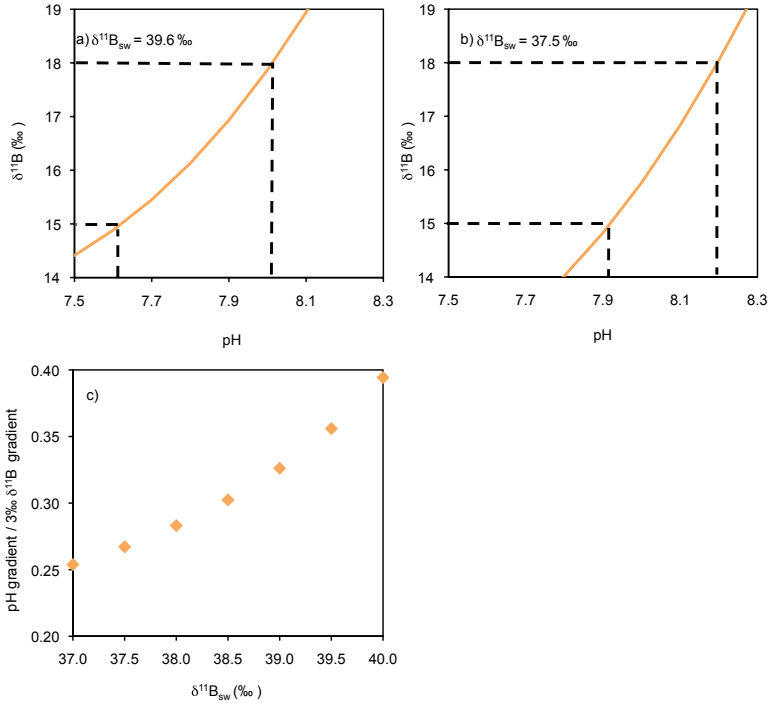

Clim. Past Discuss., doi:10.5194/cp-2015-177, 2016
Manuscript under review for journal Clim. Past
Published: 26 January 2016


Climate of the Past
Discussions
Open Access
EGU

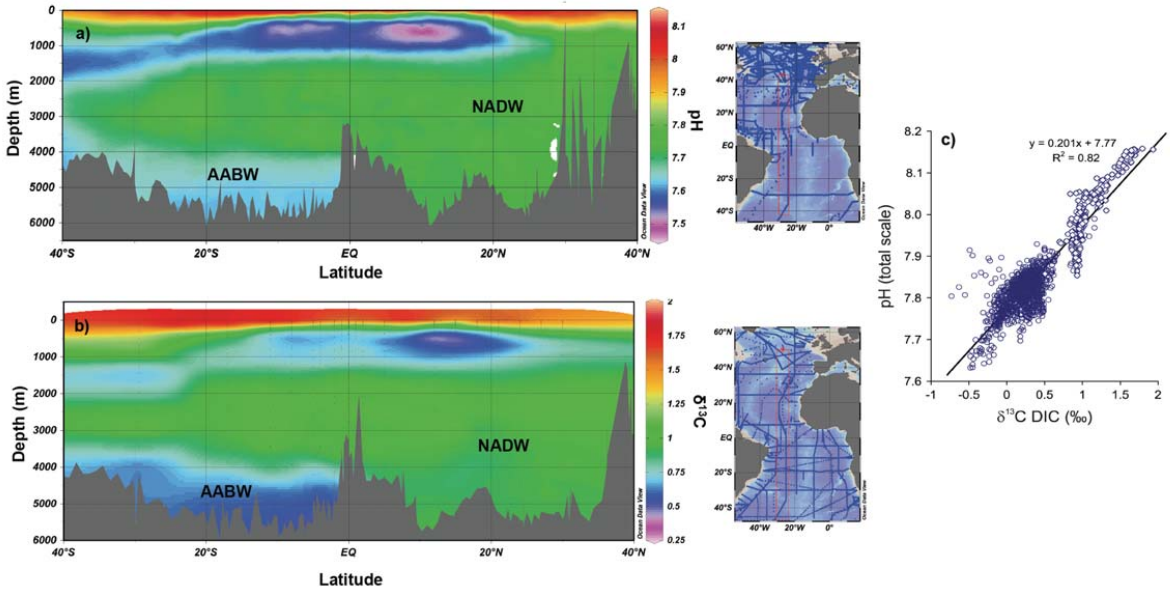

Clim. Past Discuss., doi:10.5194/cp-2015-177, 2016
Manuscript under review for journal Clim. Past
Published: 26 January 2016


Climate of the Past
Discussions
Open Access
EGU

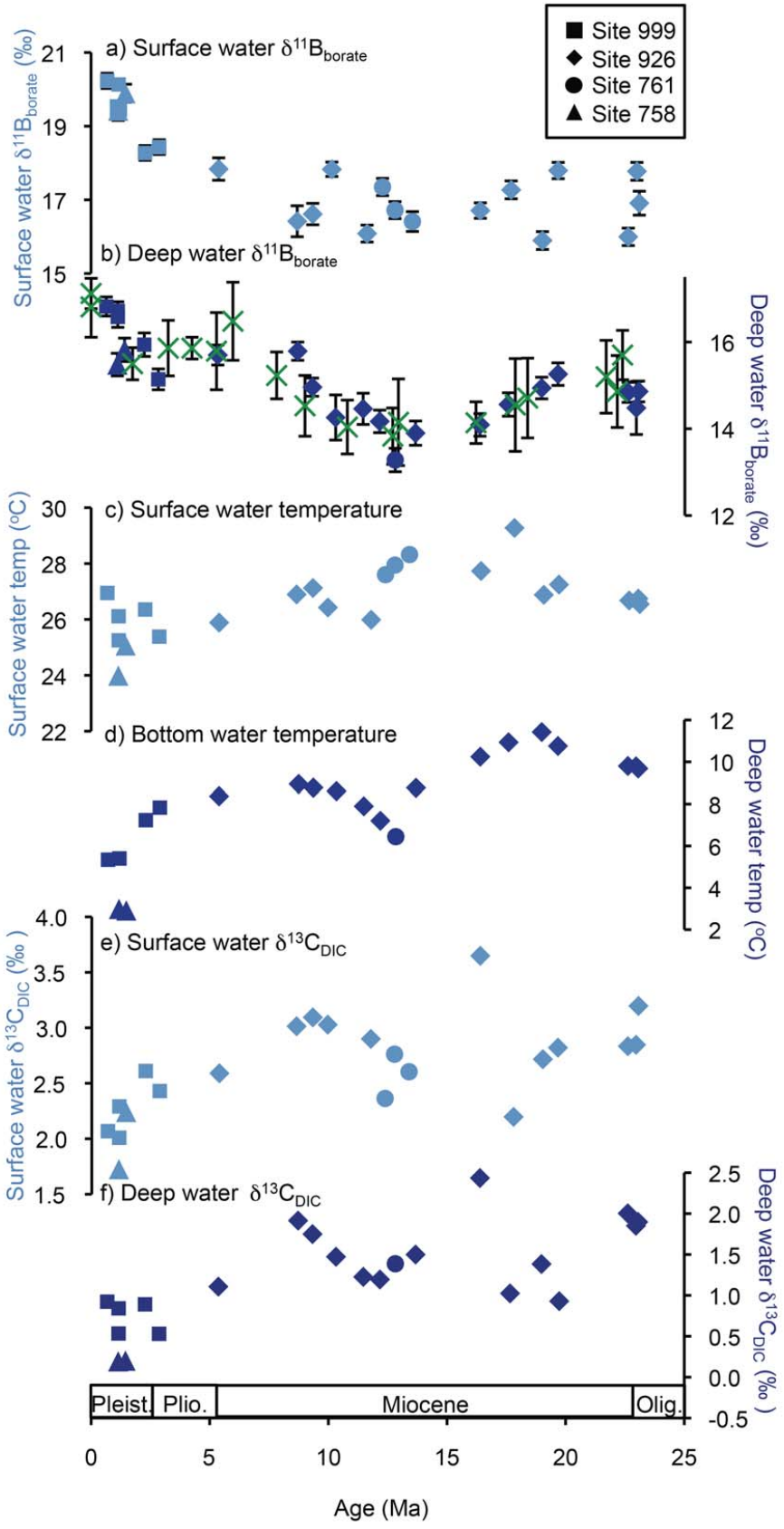

Clim. Past Discuss., doi:10.5194/cp-2015-177, 2016
Manuscript under review for journal Clim. Past
Published: 26 January 2016


Climate of the Past
Discussions
Open Access
EGU

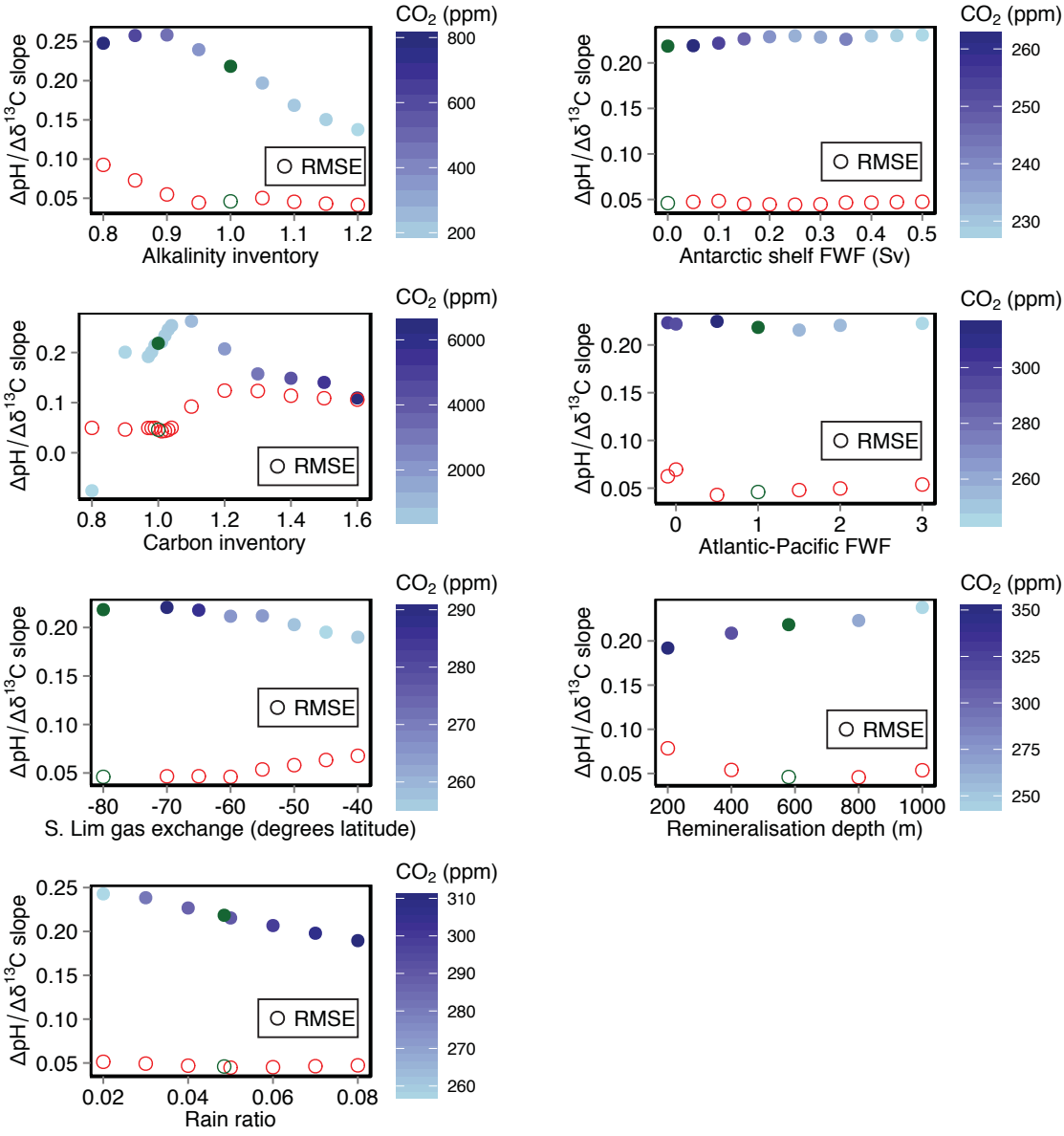

Clim. Past Discuss., doi:10.5194/cp-2015-177, 2016
Manuscript under review for journal Clim. Past
Published: 26 January 2016


Climate of the Past
Discussions
Open Access
EGU

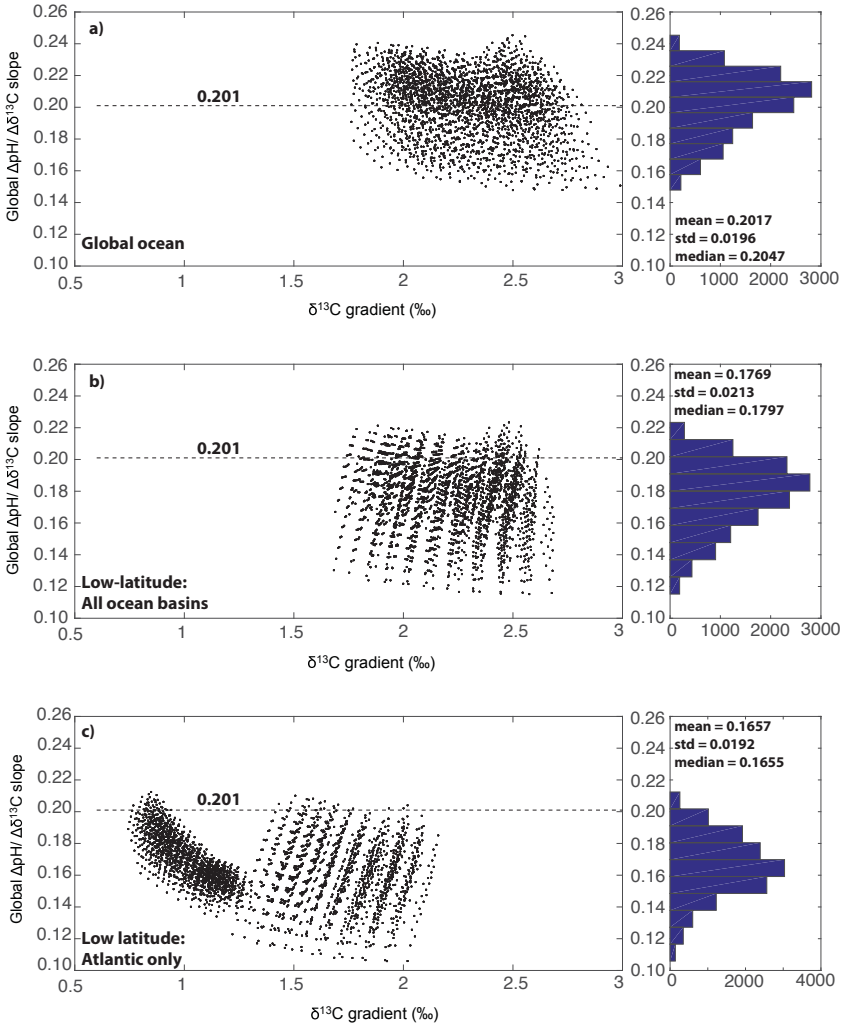

Clim. Past Discuss., doi:10.5194/cp-2015-177, 2016
Manuscript under review for journal Clim. Past
Published: 26 January 2016


Climate of the Past
Discussions
Open Access
EGU

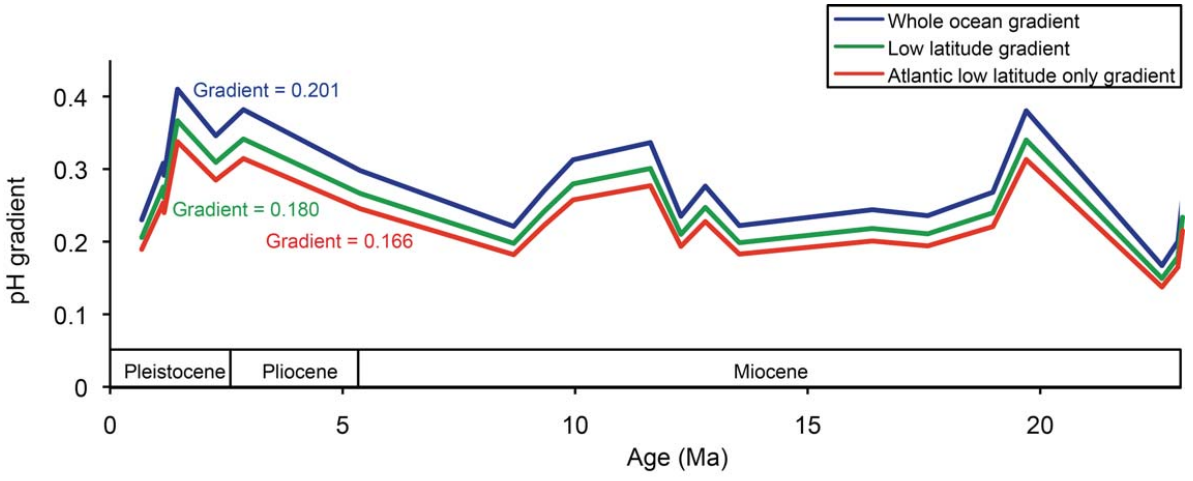

Clim. Past Discuss., doi:10.5194/cp-2015-177, 2016
Manuscript under review for journal Clim. Past
Published: 26 January 2016


Climate of the Past
Discussions
Open Access
EGU

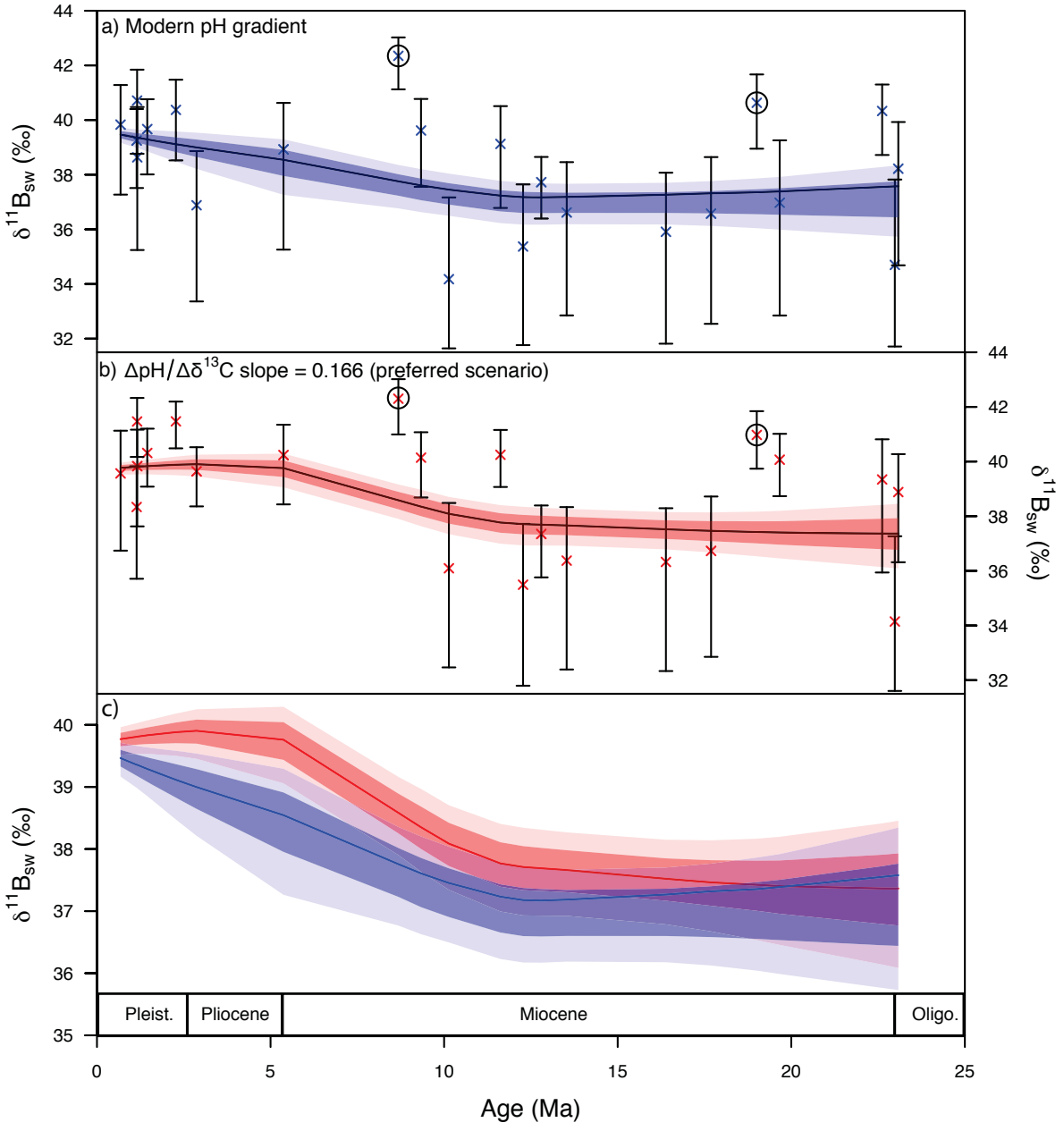

Clim. Past Discuss., doi:10.5194/cp-2015-177, 2016
Manuscript under review for journal Clim. Past
Published: 26 January 2016


Climate of the Past
Discussions
Open Access
EGU

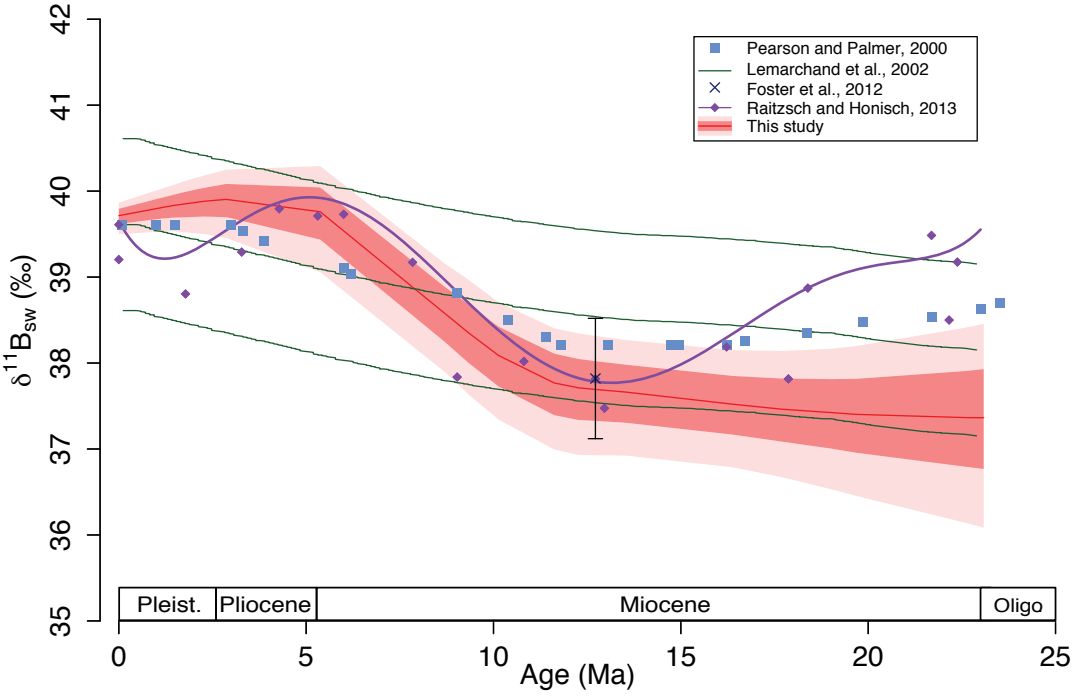

Clim. Past Discuss., doi:10.5194/cp-2015-177, 2016
Manuscript under review for journal Clim. Past
Published: 26 January 2016


Climate of the Past
Discussions
Open Access
EGU

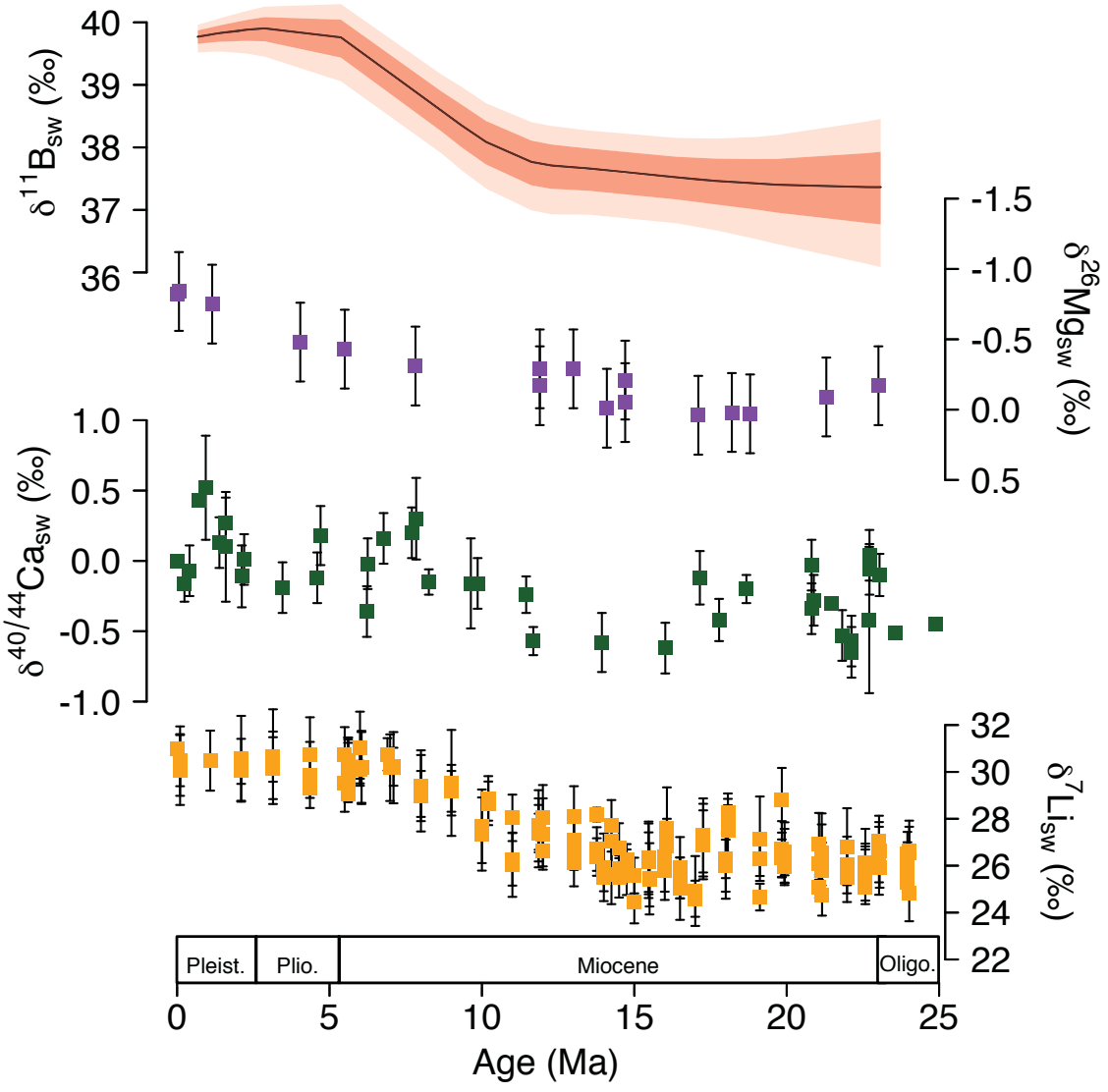

Clim. Past Discuss., doi:10.5194/cp-2015-177, 2016
Manuscript under review for journal Clim. Past
Published: 26 January 2016


Climate of the Past
Discussions
Open Access
EGU

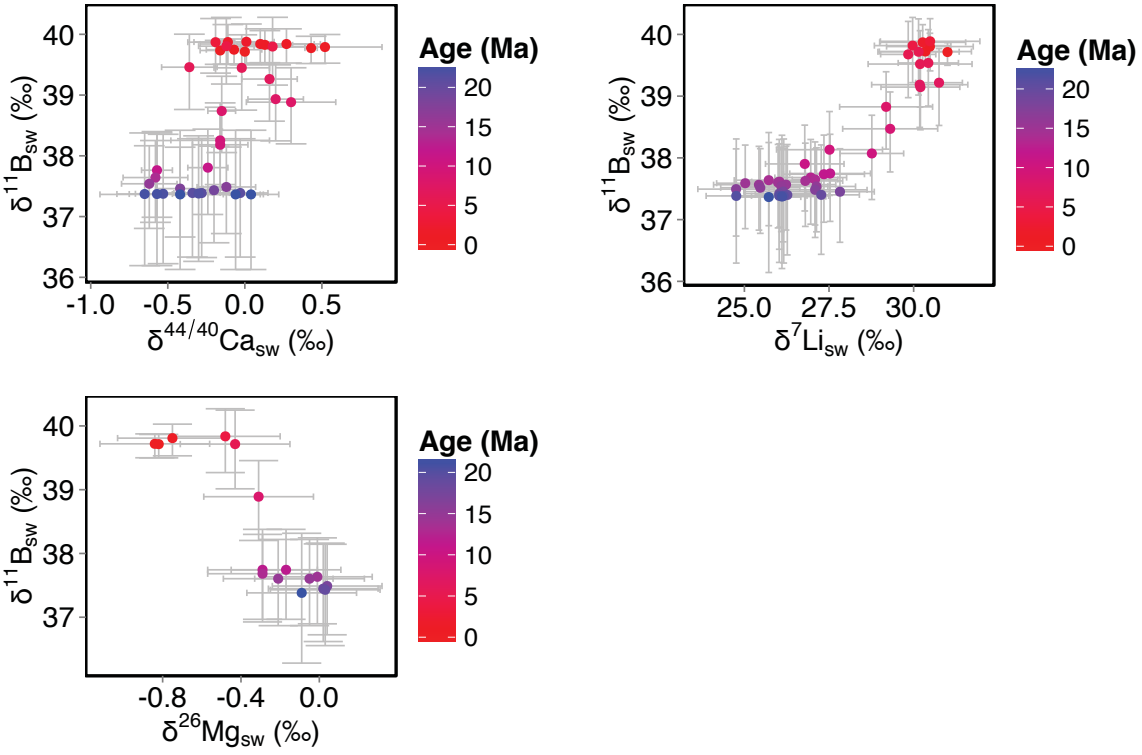

Clim. Past Discuss., doi:10.5194/cp-2015-177, 2016
Manuscript under review for journal Clim. Past
Published: 26 January 2016


Climate of the Past
Discussions
Open Access
EGU

| Sources | Isotopic Ratio | | | |
|---|---|---|---|---|
| **Oceanic Inputs** | $\delta^{11}B_{sw}$ 39.61 ‰ | $\delta^{7}Li_{sw}$ 31 ‰ | $\delta^{26}Mg_{sw}$ −0.83 ‰ | $\delta^{44/40}Ca_{sw}$ 0 ‰ |
| Input from hydrothermal | 6.5[a] | 8.3[b] | N/A | –0.96[h] |
| Fluid from accretionary prisms | 25[a] | 15[b] | N/A | N/A |
| Riverine Inputs | 10[a] | 23[b] | −1.09[d] | -1.28[h] |
| Groundwater | N/A | N/A | -0.82[d] | −1.02[i] |
| **Outputs** | | | | |
| Precipitation into carbonates | 20[a] | 29[c] | -3.5[d,e,f] | -1.15[h,j] |
| Ocean crust alteration | 4[a] | 15[b] | -0.83[d,g] | -1.2[h] |
| Absorption onto sediment | 15[a] | 15[b] | ?? | N/A |